Sub-nucleolar trafficking of Hendra virus matrix protein is regulated by ubiquitination and oligomerisation

Stephen M. Rawlinson[1*#], Tianyue Zhao[1*], Florian A. Gomez[1], Cassandra T. David[1], Christina L. Rootes[2], Patrick F. Veugelers[1,3], Ashley M. Rozario[4], Cameron R. Stewart[2], Toby D.M. Bell[3] and Gregory W. Moseley[1#]

[1] Department of Microbiology, Biomedicine Discovery Institute, Monash University, 19 Innovation Walk (Bldg 76), Clayton Campus, Victoria 3800, Australia.

[2] CSIRO Health & Biosecurity, Australian Centre for Disease Preparedness, Geelong, Victoria, Australia.

[3] School of Chemistry, Monash University, Clayton, Victoria 3800, Australia.

[4] Department of Rural Clinical Sciences, La Trobe Institute for Molecular Science, La Trobe University, Bendigo, Victoria 3552, Australia.

* SMR and TZ contributed equally to this work.

Correspondence should be addressed to: SMR (stephen.rawlinson@monash.edu) and GWM (greg.moseley@monash.edu).

ABSTRACT

Hendra virus (HeV) is a highly pathogenic member of the Henipavirus genus (order *Mononegavirales*), the replication cycle of which occurs primarily in the cytoplasm. The HeV matrix protein (HeV M) plays critical roles in viral assembly and budding at the plasma membrane, but also undergoes nuclear/nucleolar trafficking, to accumulate in nucleoli early in infection and, later, localise predominantly at the plasma membrane. Previously we found that HeV M protein targets specific sub-nucleolar compartments (corresponding to the FC-DFC (fibrillar centre (FC)/dense fibrillar component (DFC)) where it interacts with the nucleolar protein Treacle and modulates rRNA biogenesis by subverting the host nucleolar DNA damage response, indicating the importance of specific sub-nucleolar trafficking to infection. However, the mechanisms underlying targeting and movement between sub-nucleolar compartments by viral or cellular proteins remain poorly defined. Here, we assessed the molecular regulation of HeV M protein nucleolar/sub-nucleolar trafficking, finding that in infected cells and in cells expressing HeV M protein alone, M protein localizes into Treacle-enriched FC-DFC at early time points, and that FC-DFC localization is subsequently lost due to relocalization into the surrounding granular component (GC) of the nucleolus. Analysis using mutated M proteins and pharmacological modulation of ubiquitination indicate that this dynamic localization is regulated by ubiquitination and oligomerisation, with ubiquitination required for retention of HeV M in Treacle-enriched sub-nucleolar compartments, and oligomerisation required for egress. To our knowledge, this study provides the first direct insights into the dynamics and mechanisms of viral protein trafficking between sub-nucleolar compartments, important to the interplay between HeV M protein and host cell factors during infection.

AUTHOR SUMMARY

Henipaviruses, including Hendra (HeV) and Nipah viruses, cause deadly diseases in humans and livestock and are considered priority diseases by the World Health Organization due to their epidemic potential and lack of effective treatments. Understanding how these viruses interact with host cells is essential for developing new therapeutics. Our study examines the matrix (M) protein of henipaviruses and its interaction with the nucleolus, a cell structure that mediates ribosome production, and is a common target for various viruses, although their functions are largely unresolved. Previously, we showed that the HeV M protein targets a sub-nucleolar structure, called the FC-DFC, to modulate ribosome biogenesis. Here, we report that the M protein's movement between sub-nucleolar compartments is controlled by two processes: ubiquitination, which causes accumulation of the protein in the FC-DFC, and oligomerization, which is associated with exit. Similar mechanisms are also observed in other henipaviruses. Our findings reveal mechanisms regulating the hijacking of host cell functions by henipaviruses and suggest new potential targets for antiviral therapies. This study is the first to investigate how viral proteins move within the nucleolus, offering new insights into interactions that may be significant to multiple viruses.

INTRODUCTION

The nucleolus comprises a highly multifunctional structure with long established roles in ribosome biogenesis, as well as roles in cell cycle regulation, the DNA damage response (DDR), cellular stress responses, and signal recognition particle assembly [1, 2]. The nucleolus was recently shown to be a membrane-less organelle (MLO) comprising at least three immiscible liquid condensates that are formed by liquid-liquid phase separation (LLPS) [3]. The three components are the fibrillar

67 centre (FC), dense fibrillar component (DFC) and granular component (GC). The FC is surrounded
68 by the DFC to form functional units (FC-DFC), which are embedded within the GC (Fig. 1A) [4].
69 These compartments play distinct roles, including assembling a pipeline for the key steps of
70 ribosome biogenesis.
71
72 Consistent with its multifunctionality, the nucleolus is a common target of diverse viruses [5-7].
73 This targeting is proposed to enable viral exploitation of diverse processes to usurp host cell
74 biology and/or facilitate virus replication [5-7]. Despite the prevalence of viral protein nucleolar
75 targeting, functional outcomes generally remain poorly understood. The potential nucleolar
76 functions of viral proteins are of particular interest with respect to RNA viruses that typically have
77 limited coding capacity and replicate their genomes in the cytoplasm, but nevertheless target
78 specific proteins to nucleoli. These include the highly pathogenic non-segmented negative sense
79 RNA viruses (nsNSVs) Hendra (HeV) and Nipah (NiV) viruses (genus *Henipavirus*, family
80 *Paramyxoviridae*), the matrix (M) protein of which localizes to the nucleus and nucleolus during
81 infection [8-11].
82
83 Henipavirus M proteins form stable homodimers, and play critical roles in virus assembly in the
84 cytoplasm and in budding at the plasma membrane, which involves the formation of M protein
85 oligomers [12, 13]. The subcellular localization of M protein is dynamic, being nucleolar early in
86 infection before exiting the nucleolus/nucleus and accumulating at the plasma membrane for
87 assembly/budding [8-11]. Interestingly, transit through the nucleolus is reported to be a
88 prerequisite for M protein to fulfill assembly and budding functions, suggestive of a regulatory
89 role of nucleoli in viral release [10, 11]. Genetic screens have indicated the importance of nucleolar

90 proteins in infection, and proteomic datasets suggest that M protein interacts with multiple
91 nucleolar proteins [8, 10, 14, 15]. However, potential intranucleolar roles of HeV M protein
92 remained unresolved until the identification of a novel nucleolar function whereby HeV M
93 localises to a sub-nucleolar compartment corresponding to the FC-DFC, where it interacts with
94 Treacle protein and impairs ribosomal RNA (rRNA) biogenesis [14]. This process appears to be
95 mediated by mimicry of a cellular process that normally occurs during a DDR. Thus subcellular
96 trafficking underpins key functions of HeV M. However, how this trafficking is regulated,
97 particularly between sub-nucleolar compartments and other regions of the cell remains unresolved.
98 Indeed, the mechanisms regulating trafficking of proteins in general between sub-nucleolar liquid
99 condensates is poorly understood, with no prior studies to our knowledge, for any viral protein.
100
101 Previously we showed that substitution of residue K258 in HeV M for alanine (HeV M K258A)
102 impairs FC-DFC localisation/Treacle-binding and DDR modulation/budding activity, without
103 preventing localization to the GC, where HeV M K258A accumulates [14]. K258 forms part of a
104 bipartite nuclear localization sequence (NLS; often referred to as 'NLS2'; M contains at least two
105 NLSs; NLS1 is located at residues 82-87 [16, 17]) and is reported to be required for M
106 ubiquitination (Fig. 2A) [10, 11]. It has been proposed that the M protein enters the nucleus via
107 the NLS and accumulates within nucleoli before exiting the nucleolus and nucleus (mediated by a
108 nuclear export sequence (NES)). Exit of the nucleolus/nucleus is reported to be triggered by
109 ubiquitination requiring K258 by an unidentified ubiquitin ligase [18]. However, this model was
110 proposed prior to the description of the functionally important localization of HeV M to sub-
111 nucleolar compartments. As a result, the coordination and regulation of various trafficking steps,
112 including trafficking within the nucleolus, remain undefined.

113

114 The potential role of ubiquitination, and definition of other molecular mechanisms in sub-nucleolar
115 localization are of particular interest as mechanisms regulating nucleolar/sub-nucleolar trafficking
116 (which involves movement between LLPS structures) are poorly understood compared with those
117 for nuclear trafficking, which involves conventional protein interactions with trafficking receptors
118 and the nuclear pore complex. In this study, we examined the regulation of HeV M protein
119 trafficking between the FC-DFC and GC finding that ubiquitination plays a crucial role.
120 Interestingly, our data indicate that ubiquitination exerts opposing effects on sub-nucleolar and
121 nucleocytoplasmic localization, suppressing exit from the FC-DFC to the GC while being required
122 for egress from the nucleolus/nucleus. Furthermore, mutations affecting HeV M oligomerization
123 indicated that oligomerization is necessary for FC-DFC egress. These findings provide new
124 insights into the interplay of ubiquitination and oligomerization in HeV M protein
125 nuclear/nucleolar transit and roles in modulation of host cell biology, viral assembly and budding.

126 **RESULTS**

127 ***Ubiquitination affects sub-nucleolar trafficking of HeV M protein.***

128 Previously HeV M protein was reported to be ubiquitinated at several sites, potentially including
129 residue K258 (and equivalent residues in other henipaviruses), and that mutation of K258 to A or
130 R (the latter preventing ubiquitination but retaining the positive charge) inhibits ubiquitination of
131 several sites that were shown to be mono-ubiquitinated [10, 11]. Ubiquitination was implicated in
132 M protein trafficking using the proteasome/ubiquitination inhibitor, MG132, which caused nuclear
133 and nucleolar retention of HeV and NiV M proteins, and inhibited nuclear export and viral-like
134 particle (VLP) production by NiV M proteins [10, 11].

135

136 To explore the possibility that ubiquitination regulates trafficking between sub-nucleolar
137 condensates, we examined the effect of MG132 treatment on localization/accumulation of HeV M
138 protein to sub-nucleolar punctate compartments (which correspond to FC-DFC; Fig. S1 and data
139 previously reported data [14]) using confocal laser scanning microscopy (CLSM) analysis of living
140 HeLa cells expressing GFP-fused wild-type (WT) HeV M (GFP-HeV M). GFP-HeV M
141 accumulated with FC-DFC (Fig. 1B). Notably, FLAG-tagged HeV M protein also localised within
142 FC-DFC (Fig. S2A) and interacted with Treacle (Fig. S2B), but not with the Treacle-binding
143 mutant (K258A), as expected [14], suggesting that the GFP-tag is not causing artefacts.

144

145 As expected [10, 11], MG132 treatment resulted in an apparent increase in nuclear accumulation
146 of GFP-HeV M protein (Fig. 1B); quantitative image analysis confirmed a significant increase in
147 the nuclear to cytoplasmic fluorescence ratio (Fn/c) (Fig. 1C). This is consistent with previously
148 reported impairment of nuclear export [10, 11]. In contrast, accumulation of M protein in the FC-

149 DFC appeared to be reduced (Fig. 1B), and this effect was confirmed by a reduced ratio of
150 fluorescence intensity of the FC-DFC compared with the GC ($F_{FC\text{-}DFC/GC}$) (Fig. 1D), an increase in
151 GC fluorescence indicative of movement of M protein from the FC-DFC into the surrounding GC
152 (Fig. 1E), and a decrease in the number of cells with FC-DFC accumulation of M protein (Fig.
153 1F).
154
155 To confirm that the effects of MG132 on HeV M sub-nucleolar trafficking are due to
156 ubiquitination, we co-transfected cells with a plasmid expressing HA-ubiquitin (HA-Ubi) to
157 replenish ubiquitin depletion by MG132. Expression of HA-Ubi reversed the effect of MG132 in
158 reducing FC-DFC accumulation in a dose-dependent fashion (Fig. 1G, H). These findings indicate
159 that ubiquitination promotes the accumulation of HeV M protein within the FC-DFC, while
160 reduced ubiquitination leads to its egress from the FC-DFC and accumulation in the GC. The
161 observed increase in GC fluorescence is consistent with previous reports of an apparent
162 enhancement of nuclear and nucleolar localization of M protein following MG132 treatment,
163 proposed to reflect decreased export from the nucleus and corresponding decrease in egress from
164 the nucleolus[10]. Our data suggest that the accumulation of diffuse (GC) fluorescence in the
165 nucleolus following MG132 treatment is not solely due to reduced nuclear/nucleolar egress, but
166 also increased egress from the FC-DFC to the GC. Notably, the opposing effects of ubiquitination
167 on FC-DFC and nuclear/nucleolar GC localization indicate different mechanisms affecting
168 trafficking between the compartments, such that FC-DFC localization is not simply the result of
169 altered protein concentration in the nucleus/nucleolar compartment, but is specifically and
170 distinctly regulated by ubiquitination.
171

172 Previously, proteosome inhibitors were shown to reduce NiV titers during live virus infections,
173 indicating that ubiquitination plays a critical role in NiV infection [11]. To test if similar
174 mechanisms occur during HeV infection, HeLa cells were infected with HeV at MOIs of 0.5 or 5,
175 followed by treatment with proteosome inhibitors MG132 (Fig. 1I) and Bortezomib (Fig. 1J). Both
176 inhibitors reduced virus titers in a dose-dependent manner at both MOIs, with statistically
177 significant effects at both MOIs for Bortezomib and at MOI 0.5 MG132; the reduction observed
178 for MG132 at MOI 5 was dose-dependent but not significant. These findings confirm the
179 importance of ubiquitination in HeV infection, similar to what is observed with NiV [11].
180
181 ***Conservative substitution of K258 to R reduces FC-DFC targeting by HeV M.***
182 We previously showed that K258A mutation in HeV M protein (HeV M K258A) abolishes its
183 targeting to the FC-DFC, resulting in accumulation within the GC and loss of binding to the FC-
184 DFC-enriched protein, Treacle [14]. This suggested that K258 forms part of a targeting signal due
185 to its positive charge and/or affects sub-nucleolar localization due to its ubiquitination [10, 11].
186 The above data (Fig. 1) indicate that ubiquitination is required for the retention of HeV M within
187 the FC-DFC. Mutation at K258 is reported to affect mono-ubiquitination at several sites, which
188 has been suggested to indicate ubiquitination likely occurs at K258 but also impacts on other
189 mono-ubiquitination sites in M protein [11]. To examine whether the effects we observed on FC-
190 DFC localization following MG132 relate to ubiquitination at K258 or associated sites, we
191 compared the effects on subcellular localization of HeV M by the substitutions K258A (which
192 removes the positive charge and the potential ubiquitination site) and K258R (which retains a
193 positive charge but lacks the lysine of the potential ubiquitination site) (Fig. 2A). Previous studies
194 on equivalent mutations in NiV M protein indicated that the positive charge is important to

195 function of the nuclear localization sequence (NLS) and nucleolar accumulation, while
196 ubiquitination regulates nuclear export [11]. However, no effects on sub-nucleolar localization was
197 reported, although our data indicate that ubiquitination has opposing effects on nuclear/nucleolar
198 accumulation and FC-DFC accumulation (above).
199
200 CLSM analysis of cells expressing GFP-fused HeV M WT, K258A or K258R variants (Fig. 2B),
201 indicated sub-nucleolar accumulation of WT M protein in c. 90% of cells, consistent with
202 localization to FC-DFC (Fig. 2C). As expected [14], HeV M K258A protein did not
203 localize/accumulate within FC-DFC, but accumulated within the GC in 100% of cells (Fig. 2B).
204 In contrast, HeV M K258R displayed an intermediate phenotype, with a substantial proportion of
205 cells (c. 60%) showing FC-DFC accumulation similar to WT and the remainder lacking FC-DFC
206 accumulation similar to K258A (Fig. 2B, C). Consistent with this, the $F_{FC\text{-}DFC/GC}$ ratio for HeV M
207 K258A (c. 1.0) was significantly lower than that for HeV M WT (c. 1.8), while HeV M K258R
208 showed an intermediate phenotype (c. 1.4) (Fig. 2D). The reduced $F_{FC\text{-}DFC/GC}$ for HeV M K258R
209 resulted from the presence of a K258A-like sub-population (for which the $F_{FC\text{-}DFC/GC}$ was
210 equivalent to that for K258A) and the fact that the $F_{FC\text{-}DFC/GC}$ for the population with apparent FC-
211 DFC accumulation was significantly lower than the $F_{FC\text{-}DFC/GC}$ for HeV WT protein ($p < 0.01$)
212 (Fig. 2D); thus, even in cells where HeV M K258R localized to the FC-DFC, this localization was
213 impaired compared with the HeV M WT protein. Overexpression of HA-Ubi, treatment with
214 MG132, or a combination of these conditions did not result in any significant FC-DFC
215 accumulation of HeV M K258A (Fig. 2E, F), consistent with the positive charge at residues 258
216 being essential for FC-DFC localization [14]. Interestingly, MG132-treatment of cells expressing
217 GFP-HeV-M-K258R resulted in a significant reduction in FC-DFC accumulation to reach levels

218 similar to HeV M K258A, and HeV M WT with MG132/HA (Fig. 1H). Expression of HA-Ubi
219 reversed this effect (Fig. 2G, H). Together, these data imply that ubiquitination dependent on K258
220 is required for efficient FC-DFC localization, but that ubiquitination at other K258-independent
221 sites (either in M protein or other cellular proteins), is also required.
222
223 ***Dynamic localization of HeV M in sub-nucleolar compartments is regulated by K258.***
224 The effects of the K258 mutation on HeV M protein accumulation in FC-DFC suggest potential
225 impacts on a targeting sequence and/or affinity for specific components within the FC-DFC. For
226 NiV M protein, K258 is proposed to be part of a NLS, which typically consists of short stretches
227 of basic residues. Several basic residues (R244, R245, R256, R257, K258 in NiV M) are highly
228 conserved among henipavirus M proteins [10, 11]. Thus, K258 may play a crucial role in nuclear
229 import through the NLS and contribute to an overlapping targeting sequence for nucleoli/sub-
230 nucleolar FC-DFC [11, 17]. Previous data indicated that ubiquitination dynamically regulates the
231 nuclear localization of HeV M [10]. Moreover, NiV M protein undergoes dynamic and temporal
232 regulation of localization during infection, being nuclear/nucleolar early in infection before
233 nucleolar exit/nuclear export, and eventual accumulation and budding at the plasma membrane [9,
234 11]. Similarly, we found that in HeV-infected cells, HeV M localizes to sub-nucleolar
235 compartments (FC-DFC) early during infection (7 hours post-infection (p.i.)), but becomes more
236 diffuse in the nucleolus (i.e. accumulated into the GC), and with greater nuclear accumulation at
237 24 hours p.i. (Fig. 3A), consistent with observations for GFP HeV M WT protein and observations
238 of dynamic nuclear/nucleolar localization of M protein in NiV infected cells [11]. Thus, we
239 speculated that the observed differences in FC-DFC localization between HeV M WT and the
240 K258 mutants (assessed at 24 hours post-transfection in Fig. 1 and Fig. 2) might be attributable to

241 the dynamic regulation of various M protein trafficking signals related to the changes in HeV M
242 localization during infection.
243
244
245 To investigate this, we assessed the sub-nucleolar localization of HeV M WT and mutant proteins
246 at time points from 8 h to 72 h p.t. (Fig. 3B-D). The WT HeV M protein exhibited clear
247 accumulation in FC-DFC (typically multiple structures in each nucleolus) at 8 h p.t. (c. 85% of
248 cells), which progressively diminished over the course of the experiment, accompanied by a more
249 diffuse GC distribution with only around 10% of cells exhibiting accumulation of M protein in
250 multiple FC-DFC at 72 h p.t. (Fig. 3E). This is consistent with a dynamic interaction whereby M
251 protein initially enters the FC-DFC and then undergoes gradual egress to the GC. Measurement of
252 the $F_{FC\text{-}DFC/GC}$ confirmed a progressive loss of FC-DFC localization (Fig. 3F).
253
254 Consistent with roles of K258 in NLS activity of NiV M protein [10], the Fn/c for HeV M K258A
255 was reduced compared with WT at 8 and 16 h p.t., supporting its involvement in nuclear import
256 (Fig. 3G; Fn/c c. 2 for WT, compared with Fn/c c. 1 for K258A at both timepoints). Further
257 analysis revealed that the reduction in nuclear localization of the K258A mutant was due to a
258 significant proportion of cells with higher fluorescence intensity in the cytoplasm (Fc) than in the
259 nucleus (Fn) at early time points, in contrast to cells expressing WT and K258R M protein (Fig.
260 3H; c. 50-60% of cells expressing K258A M protein showed Fn > Fc between 8-24 h p.t., whereas
261 in cells expressing WT M protein, > 85% of cells showed Fn > Fc at all timepoints). However,
262 over time, the K258A mutant gradually exhibited a proportion of cells with Fn > Fc similar to WT

263 and K258R (nearly 100% of cells at 48 and 72 h p.t.), suggesting a delay in nuclear import of
264 K258A compared to the other variants.
265
266 Despite reduced nuclear accumulation at early time points, HeV M K258A was strongly nucleolar
267 at all time points, consistent with reduced nucleolar egress. However, no accumulation in FC-DFC
268 was observed at any time point, and some images indicated absence of fluorescence from these
269 structures (e.g. white arrow, 48 h p.t., Fig. 3C). Thus, HeV M protein can specifically partition
270 between sub-nucleolar phase-separated compartments, dependent on K258, and this is independent
271 of the accumulation in the nucleus, consistent with distinct mechanisms of trafficking/localization.
272 Notably, similar dynamics were observed for WT NiV M, with the percentage of cells showing
273 FC-DFC accumulation reducing over time (c. 25% of cells showing FC-DFC accumulation at 72
274 h p.t.), while NiV M-K258A remained excluded from FC-DFC at all timepoints (Fig. S3).
275
276 HeV M K258R accumulated to higher levels in the nucleus than the cytoplasm at early time points
277 compared with K258A (Fig. 3D, upper panels and 3G), similar to WT M. This is consistent with
278 a requirement for the positive charge in the NLS for efficient nuclear import, as reported for NiV
279 M protein [11, 17]. Additionally, HeV M K258R accumulated to very high levels in the nucleus
280 at later time points (48 h), consistent with an impaired nuclear export mechanism [10, 11]. HeV
281 M K258R also showed clear FC-DFC localization in Treacle-enriched compartments at 8 h p.t.
282 (Fig. 3D), similar to (but moderately reduced compared with) WT HeV M protein, followed by
283 loss of FC-DFC localization over time. Thus, the presence of a basic residue at position 258 is
284 necessary for initial entry and accumulation within the FC-DFC.
285

286 While FC-DFC localization of WT and K258R HeV M protein diminished following the initial
287 accumulation, the apparent rate of loss was greater for HeV M K258R, such that by 24 h p.t. (Fig.
288 3E) c. 25% of HeV M K258R-expressing cells displayed FC-DFC localization compared with c.
289 60% for WT HeV M. By 48 and 72 h p.t. < 5% and 0%, respectively, of HeV M K258R-expressing
290 cells displayed FC-DFC localization, and nucleoli with apparent exclusion from FC-DFC
291 structures were apparent (e.g. 48 h p.t., Fig. 3D, white arrow, similar to observations for HeV M
292 K258A. Calculation of the $F_{FC\text{-}DFC/GC}$ ratio confirmed a significant decrease in FC-DFC
293 localization by both HeV M WT and K258R over the course of the experiment, with a more rapid
294 decrease for the latter (Fig. 3F). Thus, it appears that HeV M localises initially to the FC-DFC,
295 dependent primarily on the presence of a positive charge at position 258. HeV M then relocalizes
296 to the GC, and this process is accelerated in HeV M containing the K258R substitution that is
297 impaired for ubiquitination, consistent with ubiquitination supporting retention into the FC-DFC.
298

299 ***FC-DFC accumulation is enhanced by inhibition of HeV M protein oligomerization.***

300 Protein oligomerization has been associated with regulation of subcellular localization, including
301 nuclear import and export of proteins such as p53 [19] and signal transducer and activator of
302 transcription (STAT) proteins [20]. Moreover, oligomerization is implicated in the formation of
303 MLOs through LLPS [21, 22]. Based on the crystal structure of HeV M protein, residue R57 of
304 HeV M has been implicated in oligomerization *via* packing of HeV M dimers [13]. Mutation of
305 R57 to D or E impairs the formation of VLPs by M protein, suggesting roles for oligomerization
306 in the assembly and budding processes [13]. Assembly and budding is also dependent on K258
307 [10, 11], suggesting that nuclear and nucleolar localization/trafficking, and budding are
308 intrinsically linked and/or involve coordinated regulation. Additionally, it has been hypothesized

309 that ubiquitin modification at K258 may be necessary for M protein oligomerization [18].
310 However, roles of oligomerization in HeV M nuclear/nucleolar trafficking have not been
311 investigated.
312
313 To examine this we analysed the localisation of HeV M WT or R57D as above, which indicated
314 pronounced accumulation of HeV M R57D into the FC-DFC compared to the WT protein (Fig.
315 4A). The Fn/c was not significantly different between HeV M WT and R57D indicating similar
316 function of the nuclear trafficking signals (Fig. 4B). However, the ratio of nucleolar to nuclear
317 fluorescence (Fnu/n) (Fig. 4C) and $F_{FC\text{-}DFC/GC}$ (Fig. 4D) was significantly increased for HeV M
318 R57D compared to WT HeV M protein. Thus, R57D enhances the accumulation of HeV M in the
319 FC-DFC, consistent with a role for oligomerization in regulating the localization of HeV M to
320 nucleolar condensates. These data further indicate that the mechanisms underlying M protein FC-
321 DFC localization differ from those regulating nuclear import/export. Interestingly, in contrast to
322 results for WT M protein, MG132 treatment did not reduce FC-DFC accumulation (Fig. 4E, F).
323 This suggests that the impaired ability of HeV M R57D protein to oligomerize both enhances FC-
324 DFC localization, and causes it to become insensitive to the effects of reduced ubiquitination.
325 These data are consistent with egress of M protein from the FC-DFC being dynamically regulated
326 by ubiquitination, but also being dependent on the ability of M protein to undergo oligomerization.
327
328 ***Accumulation of HeV M protein in the FC-DFC correlates with inhibitory function toward***
329 ***rRNA biogenesis and with binding to Treacle.***
330 HeV M protein accumulation in FC-DFC enables subversion of the nucleolar DDR pathway
331 through targeting of Treacle. This function is strongly impaired by the K258A mutation [14].

332 R57D and K258R enhance (Fig. 4) and suppress (to a level intermediate between WT and K258A
333 protein; Fig. 2), respectively, accumulation within the FC-DFC, suggesting that
334 oligomerization/ubiquitination regulate functional FC-DFC interactions. To assess this directly,
335 we used the Click-iT RNA Imaging Kit to measure the effects of M protein and mutants on rRNA
336 biogenesis (Fig. 5A, B), and co-immunoprecipitation (co-IP) assays to assess interactions with
337 Treacle (Fig. 5C), as previously described [14, 23].
338
339 Consistent with previous findings, WT HeV M protein, but not HeV M K258A significantly
340 impaired rRNA biogenesis at 24 h p.t.; the level of inhibition was comparable with that observed
341 for rRNA silencing by Treacle knockdown (c. 20-30% inhibition) [14, 24] (Fig. 5A, B). In contrast,
342 R57D, significantly enhanced inhibition of rRNA biogenesis compared with WT M protein (c.
343 30% inhibition), consistent with strong FC-DFC localization and apparent loss of ubiquitin-
344 regulated localization. The K258R mutation resulted in a phenotype for rRNA silencing that was
345 intermediate between WT and K258A M proteins, correlating with their differing capacities to
346 localize to the FC-DFC. Notably, the ability of WT M protein to inhibit rRNA biogenesis was lost
347 by 72 h p.t. (Fig. S4), matching with dynamic loss of FC-DFC localization (Fig. 3). As expected,
348 rRNA biogenesis in cells expressing HeV M K258A was unchanged between 24 and 72 h p.t.,
349 correlating with consistent lack of localization to the FC-DFC, while R57D was found to inhibit
350 rRNA biogenesis at both 24 and 72 h p.t. (consistent with a sustained FC-DFC localization over
351 time, see below and Fig. 6). Thus, the extent of FC-DFC accumulation appears to correspond with
352 inhibition of rRNA biogenesis.
353

354 Consistent with the differing localization and functional impact of the mutated proteins, co-IP and
355 immunoblotting (IB) analysis indicated increased interaction of HeV M R57D protein with
356 Treacle, compared with WT HeV M protein (Fig. 5C; c. 1.6-fold more Treacle precipitated with
357 R57D). Furthermore, Treacle interaction of HeV M K258R was reduced compared with WT
358 protein (c. 15% of WT levels), but was greater than HeV M K258A (c. 5 %), indicating an
359 intermediate phenotype. Notably, Treacle is reported to form multiple isoforms [25], and only the
360 upper band of Treacle appeared to IP with the M proteins (Fig. 5C), perhaps indicating interaction
361 with specific Treacle isoforms. Taken together, these data indicate that FC-DFC accumulation,
362 Treacle binding, and the inhibition of rRNA biogenesis by the HeV M protein are correlated,
363 consistent with regulation of M protein function in rRNA production *via* ubiquitin and
364 oligomerization dependent FC-DFC localization/Treacle interaction.
365
366 ***Loss of HeV M FC-DFC accumulation does not relate to disruption or loss of FC-DFC.***
367 Loss of HeV M FC-DFC localization (Fig. 3) could be attributed to two possible mechanisms: (1)
368 egress of the protein from intact FC-DFC structures, or (2) depletion of FC-DFC structures through
369 events such as fusion or disassembly/disruption of the liquid bodies. To investigate these
370 possibilities, we analysed cellular FC-DFCs directly by fixation and immunostaining of cells for
371 Treacle at time points from 8-72 h p.t. to express HeV M WT, K258A, K258R, or R57D (Fig. 6A-
372 D).
373
374 In cells expressing GFP-HeV M WT protein the appearance of FC-DFCs was similar throughout
375 the experiment (Fig. 6A). At early time points, HeV M WT protein strongly colocalized with
376 Treacle in FC-DFC, but this diminished over time (indicated by a reduced percentage of cells with

377 detectable colocalization of HeV M and Treacle FC-DFCs), although multiple Treacle-enriched
378 FC-DFCs lacking HeV M association remained detectable in nucleoli (Fig. 6A, E). Thus, HeV M
379 protein appears to transit through FC-DFC, where it interacts with Treacle, before egress, with no
380 significant disruption of FC-DFC structures. As expected, HeV M K258A showed no
381 colocalization/accumulation in Treacle FC-DFC at any time point, despite the presence of multiple
382 FC-DFC. HeV M K258R protein showed similar results to WT, but with more rapid egress, as
383 expected (Fig. 3C), and no evident loss of FC-DFC (Fig. 6C, E). By 24-48 h p.t., co-localization
384 was barely detectable, similar to K258A (Fig. 6E). In contrast, HeV M R57D exhibited clear
385 colocalization with Treacle in all detectable FC-DFCs from 8 to 48 h p.t., with only a minor
386 downward trend (colocalization with FC-DFC in c. 95% of cells measured) at 72 h p.t. (Fig. 6D,
387 E). These findings are consistent with a requirement for oligomerization for HeV M protein to
388 egress the FC-DFC, and with the capability of HeV M R57D to maintain efficient rRNA silencing
389 function at 72 h p.t., by which time WT M protein has largely lost such function. Thus, it appears
390 that HeV M protein transits through intact FC-DFC, with the loss of colocalization due to
391 trafficking rather than disruption or major structural change to FC-DFC. These data further support
392 that dynamic localization of M protein to FC-DFC, and interaction with Treacle, underlie specific
393 silencing of rRNA biogenesis.
394
395 ***HeV M proteins do not affect the structure or distribution of FC-DFC.***
396 The lack of major disruption of FC-DFC during HeV M protein accumulation or egress aligns with
397 our previous findings [14]. Specifically, using single molecule localization microscopy (SMLM)
398 with direct stochastic optical reconstruction microscopy (*d*STORM) of cells immunostained for
399 Treacle, we found that HeV M WT protein accumulation in FC-DFC (24 h p.t.) does not cause

400 ‘gross’ changes to FC-DFC numbers or to the structure of FC-DFC [14]. Based on the enhanced
401 FC-DFC localization and function in rRNA silencing observed for HeV M R57D, we reasoned
402 that, if M protein does have any structural effects on FC-DFC, they would be exaggerated by
403 R57D. We thus analysed cells expressing GFP-HeV M WT, R57D or K258A protein, and cells
404 expressing GFP alone or non-transfected cells, by immunostaining for Treacle followed by
405 *d*STORM (Fig. 7A). Expression of HeV M WT, K258A (as previously [14]), K258R and R57D
406 proteins had no significant impact on the size of Treacle-labelled FC-DFC (Fig. 7B). These data
407 are consistent with specific intermolecular interactions of M protein with Treacle within FC-DFC
408 regulating rRNA biogenesis, and the duration/extent of functional modulation being controlled by
409 ubiquitination (and potentially multimerization)-dependent egress of M protein from FC-DFC.
410

411 ***Ubiquitination regulates sub-nucleolar trafficking of M proteins of multiple henipaviruses***

412 Previously, we showed that the FC-DFC accumulation, Treacle binding, and inhibition of rRNA
413 biogenesis are conserved among M proteins of multiple henipaviruses (including NiV, Cedar
414 (CedV), and Mojiang (MojV) viruses), albeit with some differences in the extent of FC-DFC
415 accumulation [23]. To determine if ubiquitin-dependence of FC-DFC accumulation is conserved
416 in different henipaviruses, we assessed the effects of MG132 as above (e.g. Fig. 1). Similar to HeV
417 M, MG132 treatment significantly impaired NiV M FC-DFC accumulation (Fig. 8A, B) and
418 reduced the percentage of cells with FC-DFC accumulation (Fig. 8C) consistent with the homology
419 of HeV and NiV M proteins (~90% amino acid identity). Consistent with our previous report [23],
420 CedV M showed the highest accumulation in FC-DFC and lowest GC accumulation of the M
421 proteins assessed; $F_{FC\text{-}DFC/GC}$ accumulation of CedV M protein was significantly reduced (but
422 remained higher than that of HeV or NiV M proteins) following MG132 treatment, and the

423 percentage of cells with FC-DFC accumulation of CedV M protein remained c. 100% (Fig. 8C).
424 MojV M showed the lowest accumulation in FC-DFC (consistent with previous data [23]),
425 resulting only a minor and non-significant reduction in $F_{FC\text{-}DFC/GC}$ (Fig. 8B); however, there was a
426 significant reduction in the percentage of cells with clear FC-DFC accumulation of MojV M
427 protein following MG132 treatment (Fig. 8D).Taken together, these data indicate conserved roles
428 of ubiquitination in regulating henipavirus M protein localization to the FC-DFC, although the
429 extent of accumulation differs between M proteins, correlating with evolutionary divergence (c.
430 61% and 60% similarity of CedV and MojV M proteins, respectively, compared with HeV M
431 protein).
432
433
434 **DISCUSSION**
435 Here we have found that HeV M protein dynamically transits through the FC-DFC, indicating that
436 the previously identified translocation through the nucleus/nucleolus involves additional sub-
437 nucleolar trafficking between LLPS structures, with the different stages of trafficking regulated by
438 post-translational modification. This transit enables regulated interactions with Treacle and other
439 host factors, enabling functional regulation of rRNA synthesis by modulating the nucleolar DDR,
440 as well as virus assembly and budding. To our knowledge, this study presents the first data on the
441 mechanisms governing the trafficking of a viral protein within sub-nucleolar LLPS structures, and
442 expands and refines the model for M protein trafficking. Specifically, we found that M trafficking
443 to FC-DFC requires a basic residue at residue 258, and that its egress from FC-DFC requires
444 oligomerization that is regulated, at least in part, by the ubiquitination status of the M protein.
445 Importantly, while ubiquitination has previously been reported to regulate nuclear and overall

446 nucleolar localization[10], indicating that ubiquitination is required for efficient nuclear export and
447 nucleolar egress, our data, in contrast indicates that ubiquitination is required for nucleolar
448 retention/accumulation into the FC-DFC. These findings highlight that localization of proteins to
449 specific sub-nucleolar compartments involves highly specific mechanisms.
450
451 Taken together, our data support a model for M protein sub-nucleolar trafficking in which (1) entry
452 of M protein dimers into the FC-DFC and functional interaction with Treacle to modulate rRNA
453 biogenesis requires a basic charge at residue 258, and (2) exit from the FC-DFC requires
454 oligomerization of the M protein within the FC-DFC. However, the retention/egress of M from the
455 FC-DFC is dynamically regulated, at least in part, by the ubiquitination status of M protein. Our
456 data support a likely role for ubiquitination of K258, but also indicate that other ubiquitination
457 sites, either within M protein or on host proteins, also contribute, as FC-DFC localization by HeV
458 M K258R protein is impaired but remains sensitive to inhibition of ubiquitination. These
459 observations are consistent with previous data indicating that M protein can be mono-ubiquitinated
460 at at least four sites, and K258R mutation inhibits ubiquitination at several of these sites (proposed
461 to include K258 itself) which is likely to contribute to the impaired FC-DFC localization of this
462 mutant. However, at least one site remains functional which may account for the residual
463 accumulation of HeV M K258R into FC-DFC that is lost following MG132 treatment [10, 11].
464 Our data are consistent with a model whereby M protein exits the FC-DFC in the form of oligomers
465 but egress is negatively regulated by ubiquitination of M protein; however, it is also possible that
466 ubiquitination of host proteins also regulates interactions with M protein required for exit.
467

468 Movement of proteins between LLPS MLO structures such as nucleolar sub-compartments does
469 not use conventional translocation processes associated with membrane-enclosed organelles (e.g.
470 movement *via* pores/channels), but rather depends on partitioning through physicochemical
471 properties and interactions with MLO-resident molecules [4, 26]. This likely accounts for the poor
472 definition of nucleolar 'targeting sequences' compared with NLS and NES motifs that form
473 specific interactions with trafficking receptor proteins (importins and exportins) [27].
474 Ubiquitination and oligomerization play important roles in the formation and regulation of LLPS
475 [28, 29], and, notably, our data indicate a potential role for oligomerization, possibly regulated by
476 ubiquitination, in coordinating M protein's interactions/localization into sub-nucleolar liquid
477 bodies. Thus, ubiquitination/oligomerisation may alter the physicochemical properties of M
478 protein or interactions with constituents of different nucleolar condensates, as well as affecting
479 importin/exportin interactions and interactions at budding sites. The differing nature of the
480 mechanisms of sub-nucleolar trafficking and nucleocytoplasmic trafficking are consistent with our
481 observations that ubiquitination has differing effects on exit from the FC-DFC to the GC, nucleolus
482 to the nucleus, and nucleus to the cytoplasm. Thus, specific orchestration of ubiquitination,
483 deubiquitination, oligomerization, and LLPS interactions may underlie appropriate temporal
484 regulation of transport between these compartments, enabling specific control of rRNA silencing,
485 virus replication, and assembly/budding, aligning with different stages of the viral life cycle [13].
486
487 As viruses typically mimic or hijack cellular processes, our findings likely have implications
488 beyond viral infection. The intricate regulation of M protein in multiple intranuclear compartments
489 is unlikely to have evolved solely to control the concentration in the cytoplasm for viral processes
490 such as assembly and budding. Rather, it suggests a specific coordination of sub-nuclear functions,

491 including DDR subversion, where M protein appears to mimic cellular NBS1 [14]. Our findings
492 on the regulation of sub-nucleolar partitioning of M protein, including roles of positively charged
493 residues (typical of nuclear/nucleolar targeting signals), ubiquitination and oligomerisation
494 identifies mechanisms that may be relevant to cellular proteins that transit sub-nucleolar
495 compartments, including those of the DDR. In the light of current advances toward therapeutic
496 modulation of cellular and viral LLPS structures [30-33], our data also has the potential to
497 contribute to novel antiviral approaches for currently incurable Henipavirus infection, and possibly
498 other nucleolus-related pathologies [34, 35].
499
500
501 **MATERIALS AND METHODS**

502 **Cell culture, transfection and treatment**

503 HEK-293T (ATCC: CRL-3216) and HeLa (ATCC: CCL-2) cells were cultured in Dulbecco's
504 Modified Eagle Medium (DMEM) supplemented with 10% Fetal Calf Serum (FCS), 2 mM
505 Glutamax, 50 U/mL Penicillin, and 50 µg/mL Streptomycin. The cells were maintained at 37 °C
506 with 5% CO_2. HEK-293T and HeLa cells were grown to 80-90% confluency before transfection
507 using Lipofectamine 2000 and Lipofectamine 3000, respectively, according to the manufacturer's
508 instructions (ThermoFisher Scientific). For free ubiquitin depletion, transfected HeLa cells were
509 treated with 50 µM MG132 or 0.5% DMSO for control at 18 h p.t. for 6 h before CLSM imaging
510 analysis. MG132 was purchased from Sigma (M7449-200UL) as a 10 mM ready-made solution in
511 DMSO. Experiments for co-expression of HA-Ubi, HeLa cells were transfected with the same
512 total amount of DNA of 2500 ng: 1000 ng of GFP-HeV M co-transfected with 1500 ng total of
513 HA-alone plasmid and/or HA-Ubi, with the HA/HA-Ubi ratio varied.
514

515 **Virus infections**

516 Wild-type HeV (Hendra virus/horse/1994/Hendra) was used for all virus work and performed at
517 the CSIRO Australian Centre for Disease Preparedness (CSIRO-ACDP) in Biosafety Level (BSL)-
518 4 laboratories. For analysis of IF, HeLa cells were seeded onto coverslips and mock- or HeV-
519 infected (MOI 5) prior to fixation at 7 h and 24 h p.i. using 4% paraformaldehyde (1h, RT) and
520 permeabilization with 0.1% TritonX-100 for 10 min. IF labelling was performed using a mouse
521 primary antibody to HeV M (1:500; developed internally (Ref#: 1805-21-1527) and an anti-mouse
522 AlexaFluor 488 secondary antibody. DNA was visualised using a DAPI.

523

524 For tissue culture infective dose ($TCID_{50}$) analysis HeLa cells were seeded into 96-well plates prior
525 to HeV-infection the next day at MOI 0.5 or 5. At 18 h p.i. cells were treated with DMSO, MG132
526 (1 nM, 10 nM or 100 nM) or Bortezomib (5 nM, 50 nM or 500 nM). At 25 h p.i., additional
527 Bortezomib was added to Bortezomib samples, as previously done for NiV[11]. At 42 h p.i.
528 supernatants were collected and $TCID_{50}$/ml was determined as previously[36].

529

530 **Constructs**

531 Mammalian cell expression of N-terminal GFP tagged HeV-M (Accession Number AEB21196.1),
532 and mutants were generated by directional cloning of the M gene cDNA into the multiple cloning
533 site of the pEGFP-C1 vector, as previously described[17]. Site-directed mutagenesis of R57D
534 residue was performed by applying QuickChange method, using *Pfu* DNA Polymerase from
535 Promega. The following oligonucleotides were used to introduce the single R57D mutation: 5'-
536 caagatctataccccaggtgcaaatgagGACaaattcaacaactacatgtacatg-3' and 3'-
537 catgtacatgtagttgttgaatttGTCctcatttgcacctggggtatagatcttg-5'. DNA sequencing was performed to

538 confirm the correct mutation. The plasmid for expression of HA-ubiquitin (HA-Ubi) has been
539 published previously [37].
540
541 **Confocal laser scanning microscopy (CLSM) and image analysis**
542 For CLSM imaging analysis, HeLa cells were seeded on 1.5 (0.17 mm) thickness glass coverslips
543 and transfected with the indicated constructs at 80-90% confluency. Imaging was performed at the
544 indicated time p.t. or 24 h p.t., if not specified. CLSM was conducted using a Nikon C1 inverted
545 confocal microscope with a 60× oil immersion objective (NA 1.4) at Monash Micro Imaging
546 Facility. Live-cell CLSM imaging was performed within a heated chamber at 37 °C.
547
548 CLSM images were analyzed using ImageJ freeware software. The mean fluorescence of the
549 nucleus (Fn), cytoplasm (Fc), nucleolus (Fnu; whole nucleolus), FC-DFC ($F_{FC\text{-}DFC}$), GC (F_{GC}), and
550 background fluorescence (Fb) were determined. After subtracting the background fluorescence
551 (Fb) from all values, the nuclear to cytoplasmic (Fn/c), nucleolar to nuclear (Fnu/n), and FC-DFC
552 to GC ($F_{FC\text{-}DFC/GC}$) fluorescence ratios were calculated. In cells where accumulation into sub-
553 nucleolar compartments was not evident (e.g., cells expressing K258A- or K258R-mutated M
554 protein), two distinct areas in the diffuse region of the nucleolus were selected to represent the
555 "FC-DFC" and the "GC" for image analysis. The F_{GC} analysis was based on images captured under
556 the same microscopy and software settings.
557
558 The percentage of cells with FC-DFC accumulation was determined by dividing the number of
559 cells showing any nucleolus with FC-DFC ≥ 1 by the total number of cells expressing the indicated
560 proteins in each sample. Data are presented as mean ± S.E.M. (standard error of the mean) or mean

561 ± SD (standard deviation), as indicated in the figure legend. Statistical analysis (Student's t-test)
562 was performed using GraphPad Prism software.
563
564 **Immunofluorescence (IF)**
565 For IF staining, cells grown on glass coverslips were washed twice gently with PBS at 24 h p.t.,
566 fixed with 4% (w/v) paraformaldehyde at room temperature (RT) for 15 min, permeabilized using
567 0.25% Triton X-100 (v/v in PBS) at RT for 5 min, and blocked with 1% bovine serum albumin
568 (BSA) in PBS at RT for 1 h. For samples expressing FLAG-M proteins, an additional 5 min
569 incubation with 5 μg/ml proteinase K was performed after fixation. The cells were then incubated
570 with primary antibody specific to either Treacle (1:100; Cat # 11003-1-AP, Proteintech), UBF1
571 (1:500; Cat# Ab244287; Abcam), Nucleolin (1:200; Cat#14574, CST), anti-FLAG (1:250;
572 Cat#F1804, Sigma) or NPM1 (1:200; Cat# 32-5200, ThermoFisher Scientific) at RT for 1.5 h.
573 Subsequently, cells were incubated with goat anti-rabbit or anti-mouse 568 AlexaFluor conjugate
574 secondary antibody (Cat # A-11011/A-11004, ThermoFisher Scientific) at a 1:1000 dilution in the
575 dark at RT for 1.5 h. DNA staining was performed using Hoechst 33342 at a 1:2000 dilution of a
576 20 mM stock solution (Cat # 62249, ThermoFisher Scientific). The cells were mounted onto
577 microscope glass slides (Lomb Scientific) using Mowiol reagent.
578
579 **5-ethnyl uridine (EU) incorporation assays.**
580 Levels of rRNA synthesis were determined using an image-based technique (Click iT RNA Alexa
581 Fluor 594 Imaging kit, Thermo-Fisher, Cat# C10330) as previously described [14, 23, 24, 38].
582 Cells were incubated for 1 h in the presence of EU before fixation in 4% paraformaldehyde at RT
583 for 12 min and permeabilization in 0.25% Triton X-100 for 5 min at RT. Samples were processed

584 according to the manufacturer's recommendations to label incorporated EU with Alexa Fluor 594.
585 DNA was labeled using Hoechst 33342. Cells were imaged by CLSM to detect labeling of nascent
586 rRNA by measuring the fluorescence intensity of Alexa Fluor 594 within nucleoli. Quantitative
587 analysis was performed using ImageJ software to determine the mean EU fluorescence of nucleoli,
588 which were identified using a combination of DNA, GFP, and transmitted light channels. Relative
589 rRNA synthesis levels were determined by measuring nucleolar EU levels of both GFP-expressing
590 and non-expressing cells from the same sample (as an internal control) and expressed as nucleolar
591 EU of GFP-expressing cells relative to non-expressing cells.
592
593 **Immunoprecipitation (IP) and immunoblotting (IB)**
594 HEK-293T cells were seeded in 6 cm dishes and transfected to express the indicated GFP-fused
595 proteins. At 24 h p.t., cells were harvested and lysed in 10 mM Tris/Cl pH 7.5, 150 mM NaCl, 0.5
596 mM EDTA, 0.5% NP-40, and 1x Protease Inhibitor Cocktail (PIC; Sigma-Aldrich
597 Cat#11697498001) for 20 min at 4°C. The lysate was cleared by centrifugation at 20,000 xg for 6
598 min at 4°C, and 10% of the supernatant was collected as the 'input' sample. The remaining lysate
599 was incubated with GFP-Trap magnetic beads (ChromoTek) as previously described for 45 min at
600 4°C on a rotary mixer [14]. The beads were then washed three times with dilution buffer (10 mM
601 Tris/Cl pH 7.5, 150 mM NaCl, 0.5 mM EDTA, 1x PIC) and resuspended in 2x SDS-PAGE sample
602 buffer to solubilize the proteins. The entire process from the addition of lysis buffer to the addition
603 of 2x SDS-PAGE sample buffer was completed in less than 1.5 h to minimize degradation of
604 Treacle, which is commonly observed (e.g. [24, 38, 39]).
605

606 Immunoprecipitates and cell lysates (input) were analyzed by SDS-PAGE and immunoblotting
607 (IB). Proteins in IP and input samples were separated on 10% SDS-PAGE gels and transferred
608 onto nitrocellulose membranes using the Bio-Rad Trans-Blot Turbo Transfer System according to
609 the manufacturer's instructions. After protein transfer, the membranes were blocked in blocking
610 buffer (5% non-fat milk in PBS with 0.1% Tween-20) at RT for 1 h, incubated with the indicated
611 primary antibodies at RT for 2 h or at 4°C overnight on a rocker, followed by incubation with
612 HRP-conjugated secondary antibodies (goat anti-rabbit or anti-mouse) at RT for 1 h. The
613 membranes were then imaged using a Gel Doc XR+ Gel Documentation System (Bio-Rad). The
614 primary antibodies used for IB were anti-Treacle (Cat # 11003-1-AP, Proteintech; 1:2000), anti-
615 GFP (Cat # 11814460001, Roche; 1:2000), and anti-β-tubulin (Cat # T8328, Sigma; 1:2000). The
616 secondary antibodies used for IB were goat anti-rabbit (Cat # AP307P) and goat anti-mouse (Cat
617 # AP308P) IgG HRP-conjugated antibodies (Merck Millipore). The Treacle bands in the IP were
618 quantitated using ImageLab (Version 6.0) software.
619

620 ***d*STORM imaging and analysis**

621 HeLa cells were fixed 24 h p.t. with 4% paraformaldehyde for 10 min then permeabilized with
622 0.1% Triton X-100 for 10 min. Fixed cells were blocked in 2% BSA/PBS for 30 min, then stained
623 with anti-Treacle primary antibodies (3 µg/ml, 1 h) and Alexa Fluor 647 conjugated secondary
624 antibodies (5 µg/ml, 45 min). Samples were imaged with a switching buffer of 100 mM
625 mercaptoethylamine (MEA) in PBS made to pH 8.5 [40]. *d*STORM imaging was performed on a
626 home-built super-resolution set-up as previously described [40, 41]. Briefly, the setup comprised
627 an inverted fluorescence microscope (Olympus IX81, 100X 1.49 NA TIRF objective) with an
628 EMCCD camera (Andor iXon). Blue laser excitation (Toptica iBeam 488 nm) was used to identify

629 GFP-positive cells. High power red laser excitation (Oxxius LaserBoxx 638 nm) was used to
630 induce reversible photoswitching of Alexa Fluor 647 fluorophores in the fixed samples. Single
631 molecule 'blinking' events were captured at 100 Hz for between 10,000 – 20,000 frames and
632 processed using rapi*d*STORM [42] to render a 2D coordinate map as the super-resolved *d*STORM
633 images of subnucleolar Treacle. For analysis, images were first smoothed in ImageJ using the
634 Gaussian Blur function (Sigma (Radius) = 0.5) to account for single molecule localization
635 precision error. Images were converted to 8-bit (greyscale values 2-255 threshold) then converted
636 into binary images. Using the "Distance Map" function in ImageJ, individual subnucleolar
637 compartments were discretized based on pixel density by applying a threshold for greyscale values
638 2-255. The "Analyse Particles" function was then used to identify and measure subnucleolar
639 compartments.
640
641 **FIGURE LEGENDS**
642
643 **Figure 1** **Ubiquitination regulates FC-DFC accumulation of HeV M and impacts on**
644 **virus production.** (A) Schematic of a nucleolus showing the three primary sub-compartments:
645 fibrillar centre (FC), dense fibrillar component (DFC) and granular component (GC). The region
646 composed of the FC and DFC compartments is referred to as the FC-DFC. (B) HeLa cells
647 transfected to express GFP-HeV M protein were treated 18 h post transfection (p.t.) with MG132
648 or without (DMSO) for 6 h before CLSM analysis. Representative images are shown for each
649 condition; yellow boxes are magnified in the zoom panel. Yellow arrowheads indicate nucleoli;
650 white arrowheads indicate localization of M protein to sub-nucleolar compartments consistent with
651 FC-DFC. Images such as those in B were analysed to determine: (C) the nuclear to cytoplasmic

652 (Fn/c) fluorescence ratio; (D) the ratio of fluorescence of the FC-DFC to that of the GC ($F_{FC-DFC/GC}$);
653 (E) the fluorescence intensity of the GC (F_{GC}) (arbitrary units (a.u.)), and (F) the % of HeV
654 M-expressing cells with apparent accumulation in FC-DFC (histogram shows the percentage of M
655 protein-expressing cells containing at least one nucleolus with evident accumulation of M protein
656 into one or more FC-DFC). Histograms for C, D and E show mean ± S.E.M., n ≥ 24 cells for each
657 condition (data from a single assay, consistent with two independent experiments); histogram in F
658 shows mean percentage ± SD from two independent assays; ≥ 73 cells for each condition. (G)
659 HeLa cells co-transfected with plasmid to express GFP-HeV M and with differing amounts of HA
660 or HA-ubiquitin (HA-Ubi) expression plasmid (1500 ng total HA/HA-Ubi plasmid transfected,
661 comprising HA-Ubi and/or HA, as indicated) and treated without (DMSO) or with MG132. (H)
662 Images such as those in G were used to calculate the $F_{FC-DFC/GC}$. Data from a single assay (n = 24
663 cells per sample), representative of two independent assays. (I, J) HeLa cells infected with HeV at
664 MOI 0.5 or MOI 5 and treated with increasing concentrations of proteosome inhibitors, (I) MG132
665 or (J) Bortezomib (Bort), prior to collection at 42 h p.i. and determination of HeV titres
666 (TCID50/ml ± S.E.M., n = 6). Statistical analysis used Student's t-test; * $p < 0.05$; ** $p < 0.01$;***
667 $p < 0.001$; **** $p < 0.0001$; ns, non-significant.
668
669 **<u>Figure 2</u>** **K258R mutation impacts sub-nucleolar trafficking of HeV M protein**. (A)
670 Schematic of the HeV M protein indicating the bipartite NLS (residues 244-258; critical basic
671 residues are in bold and underlined) and residue K258, mutation of which regulates the ubiquitin
672 status (Ubi) of M protein by removing the proposed ubiquitin site at 258, and affecting other sites.
673 Mutations used in this study are indicated (grey boxes). (B) CLSM images of living HeLa cells
674 expressing the indicated GFP-fused proteins (24 h p.t.); for HeV M WT and K258A, images are

675 representative of 90-100% of cells in > 29 fields of view; for HeV M K258R two major populations
676 (each representing c. 40-60% of the population) were observed, corresponding to either a "FC-
677 DFC accumulation" (upper panel) or "K258A-like" (lower panel) phenotype. Nucleoli are
678 highlighted by the yellow box, which is magnified in the zoom panel. White arrowheads indicate
679 accumulation within FC-DFC. (C) Images such as those in B were analysed to determine the
680 percentage of cells with clear FC-DFC accumulation of M protein (mean percentage ± SD, n = 3
681 separate assays, each sampling ≥ 119 cells). Student's t-test with Welch's correction was used to
682 determine significance; ** $p < 0.01$.) (D) Images were analysed to determine $F_{FC\text{-}DFC/GC}$ (mean ±
683 S.E.M., n ≥ 90 cells for each condition, from three independent assays; green line in K258R
684 indicates mean of all samples). The two distinct populations in the K258R sample are indicated.
685 Comparison of K258R "WT-like" population with WT samples using Student's t-test showed a
686 significant difference ($p < 0.01$). (E-H) Images of HeLa cells co-transfected to express GFP-HeV
687 M K258A (E) or K258R (G) with different amounts of HA or HA-ubiquitin-expressing plasmid
688 imaged by CLSM (as in Fig. 1G, H). Images such as these were analyzed to determine the $F_{FC\text{-}$
689 $DFC/GC}$ of K258A (F) and K258R (H) expressing cells (n ≥ 17 cells for F, and n ≥ 21 for H; data
690 from one assay, representative of two independent assays). Statistical analysis used Student's t-
691 test; * $p < 0.05$; ** $p < 0.01$; **** $p < 0.0001$; ns, non-significant.
692

693 **<u>Figure 3</u> HeV M protein undergoes dynamic localization to the FC-DFC which is**
694 **impacted by K258R mutation.** (A) HeLa cells were mock-infected or infected with HeV (MOI
695 5) prior to fixation and immunostaining for HeV M protein at 7 h and 24 h post-infection (p.i.).
696 Nuclei were detected using DAPI. Microscope settings and image correction are identical between
697 equivalent mock and HeV infected images. (B-C) HeLa cells transfected to express the indicated

698 proteins were analysed live at 8, 16, 24, 48 and 72 h p.t. by CLSM. Images representative of major
699 phenotypes are shown for each condition; yellow boxes are magnified in the zoom panel. Yellow
700 arrowheads indicate nucleoli; white arrowheads indicate accumulation of M protein in FC-DFC.
701 Images such as those in B-C were analysed to determine: (E) the percentage of M protein-
702 expressing cells with FC-DFC accumulation in any nucleolus in the cell (mean ± SD from three
703 independent assays, n ≥ 59 cells for each condition); (F) $F_{FC\text{-}DFC/GC}$ (mean ± S.E.M., n ≥ 55 cells
704 for each condition from three independent assays, except for 8 h p.t. (WT, K258A, K258R), 16 h
705 p.t. K258A, and 48 h p.t. WT samples, where data is from two assays; (G) Fn/c (mean ± S.E.M.;
706 n ≥ 24 cells) and (H) percentage of cells with Fn > Fc (mean ± SD from three independent assays,
707 except for 8 h p.t. (WT, K258A, K258R), 16 h p.t. K258A, and 48 h p.t. WT samples, where data
708 is from two assays; n ≥ 23 cells for each condition). Student's t-test was used to compare values
709 for WT and K258R at each timepoint in D and E; * $p < 0.05$; *** $p < 0.001$; **** $p < 0.0001$; ns,
710 non-significant.
711
712 **<u>Figure 4</u> R57D mutation enhances accumulation of HeV M in FC-DFC and is**
713 **insensitive to ubiquitination depletion.** (A) CLSM images of live HeLa cells expressing the
714 indicated proteins (24 h p.t.). Images are representative of 90-100% of cells in > 9 fields of view
715 from a single assay, and typical of ≥ 4 independent assays. Hoechst 33342 (blue) was used to
716 identify DNA/nuclei. Nucleoli are highlighted by the yellow box, which is magnified in the zoom
717 panel. Yellow arrowheads indicate nucleoli; white arrowheads indicate accumulation in FC-DFC.
718 (B-D). Images such as those shown in A were used to determine (B) Fn/c; (C) nucleolar to nuclear
719 fluorescence ratio (Fnu/n; Fnu is the mean fluorescence intensity for the entire area of the
720 nucleolus); (D) $F_{FC\text{-}DFC/GC}$. B, C and D show mean ± S.E.M., n ≥ 24 cells for each condition. (E)

721 CLSM images of HeLa cells expressing the indicated protein and treated without (DMSO) or with
722 MG132. (F) Images such as those in E were analysed to determine $F_{FC\text{-}DFC/GC}$ ($n \geq 14$ cells from
723 one assay; data representative of three independent assays). Statistical analysis used Student's t-
724 test; **** $p < 0.0001$; ns, non-significant.
725
726 **<u>Figure 5</u> Silencing of rRNA synthesis and Treacle-binding by HeV M protein/mutants**
727 **correlate with FC-DFC accumulation.** (A) HeLa cells were transfected to express the indicated
728 GFP-fused proteins before addition of EU reagent (23 h p.t.) for 1h, fixation (24 h p.t.), labeling
729 to detect nascent RNA (EU fluorescence) and DNA (Hoechst 33342), and imaging by CLSM. (B)
730 Images such as those in A were used to determine EU fluorescence in the nucleoli of GFP-positive
731 cells, relative to that in non-GFP expressing cells in the same sample (mean relative EU
732 fluorescence ± S.E.M., $n \geq 51$ cells from two independent experiments). * $p< 0.05$; *** $p < 0.001$;
733 **** $p < 0.0001$; ns, non-significant. (C) HEK-293T cells were transfected to express GFP or the
734 indicated GFP-fused proteins prior to lysis (24 h p.t.) and IP for GFP. Cell lysate (input) and IP
735 samples were subjected to IB using the indicated antibodies. Quantitation of Treacle band in IPs,
736 relative to that detected in IP for GFP-HeV M WT are indicated.
737
738 **<u>Figure 6</u> M protein FC-DFC accumulation decreases over time without loss of FC-DFC**
739 **compartments.** (A-D) HeLa cells were transfected to express the indicated proteins before
740 fixation at 8, 16, 24, 48 and 72 h p.t. and immunostaining using anti-Treacle antibody (red) and
741 imaging via CLSM. Hoechst 33342 (blue in Merge panels) was used to localize DNA/nuclei.
742 Representative images are shown for each condition; yellow arrowheads indicate nucleoli; unfilled
743 white arrowheads indicate Treacle in FC-DFC; white arrowheads indicate accumulation of M

744 protein into FC-DFC; yellow arrows indicate colocalization of Treacle and HeV M protein in FC-
745 DFC. (E) Images such as those in A-D were analysed to determine the percentage of cells
746 expressing HeV M protein with evident colocalization of HeV M protein and Treacle in FC-DFC
747 ($n \geq 23$ cells for each condition).
748
749 **Figure 7** **HeV M R57D protein does not affect the structure or distribution of Treacle-**
750 **enriched FC-DFC.** (A) HeLa cells expressing the indicated proteins or non-transfected (NT) were
751 fixed and immunolabeled for Treacle before imaging using SMLM with *d*STORM. Fluorescence
752 microscopy was used to identify cells expressing GFP/GFP-fusion proteins (green). Yellow boxes
753 in fluorescence images show zoomed region imaged using SMLM (Zoom 1); yellow boxes in
754 Zoom 1 images show additional zoomed region (Zoom 2). Scale bars correspond to 5000 nm
755 (Zoom 1) and 500 nm (Zoom 2). SMLM images such as those shown in A were used to determine
756 (B) Tukey boxplots showing median area and the 95% confidence interval of Treacle-enriched
757 FC-DFC ($n \geq 505$ FC-DFC for each sample). Statistical analysis used Kolmogorov-Smirnov tests
758 as normality testing indicated a non-parametric distribution.
759
760 **Figure 8** **FC-DFC accumulation of M proteins of multiple henipaviruses is regulated by**
761 **ubiquitination.** (A) CLSM images of live HeLa cells transfected to express the indicated proteins.
762 Representative images are shown for each condition, with yellow boxes magnified in the zoom
763 panel. Hoechst 33342 was used to stain nuclei/DNA. (B) Images such as those in A were used to
764 determine $F_{FC\text{-}DFC/GC}$ (mean $F_{FC\text{-}DFC/GC} \pm$ S.E.M., from one assay ($n \geq 13$), representative of three
765 independent assays). (C) The percentage of M protein-expressing cells with apparent

accumulation of M protein in FC-DFC (mean percentage ± S.E.M. from three independent assays; each sample was determined from n ≥ 13 cells).

ACKNOWLEDGEMENTS

We acknowledge the facilities and technical assistance of Monash Micro Imaging (Monash University) with confocal microscopy. This study was supported by National Health and Medical (NHMRC) Research Council grants 1125704, 1160838 and 1079211 to GWM; Australian Research Council (ARC) grants DP210100998, DP150102569 to GWM, and DP170104477 to TDMB; and the Miegunyah Trust Grimwade Fellowship to GWM.

776

777 1. Boisvert FM, van Koningsbruggen S, Navascues J, Lamond AI. The multifunctional
778 nucleolus. Nat Rev Mol Cell Biol. 2007;8(7):574-85. doi: 10.1038/nrm2184. PubMed PMID:
779 17519961.

780 2. Iarovaia OV, Minina EP, Sheval EV, Onichtchouk D, Dokudovskaya S, Razin SV, et al.
781 Nucleolus: A Central Hub for Nuclear Functions. Trends Cell Biol. 2019;29(8):647-59. Epub
782 2019/06/10. doi: 10.1016/j.tcb.2019.04.003. PubMed PMID: 31176528.

783 3. Feric M, Vaidya N, Harmon TS, Mitrea DM, Zhu L, Richardson TM, et al. Coexisting
784 Liquid Phases Underlie Nucleolar Subcompartments. Cell. 2016;165(7):1686-97. Epub
785 2016/05/24. doi: 10.1016/j.cell.2016.04.047. PubMed PMID: 27212236; PubMed Central
786 PMCID: PMCPMC5127388.

787 4. Lafontaine DLJ, Riback JA, Bascetin R, Brangwynne CP. The nucleolus as a multiphase
788 liquid condensate. Nat Rev Mol Cell Biol. 2021;22(3):165-82. Epub 2020/09/03. doi:
789 10.1038/s41580-020-0272-6. PubMed PMID: 32873929.

790 5. Hiscox JA. RNA viruses: hijacking the dynamic nucleolus. Nat Rev Microbiol.
791 2007;5(2):119-27. Epub 2007/01/17. doi: 10.1038/nrmicro1597. PubMed PMID: 17224921;
792 PubMed Central PMCID: PMCPMC7097444.

793 6. Iarovaia OV, Ioudinkova ES, Velichko AK, Razin SV. Manipulation of Cellular Processes
794 via Nucleolus Hijaking in the Course of Viral Infection in Mammals. Cells. 2021;10(7). Epub

795 2021/07/03. doi: 10.3390/cells10071597. PubMed PMID: 34202380; PubMed Central PMCID:
796 PMCPMC8303250.

797 7. Rawlinson SM, Moseley GW. The nucleolar interface of RNA viruses. Cell Microbiol.
798 2015;17(8):1108-20. doi: 10.1111/cmi.12465. PubMed PMID: 26041433.

799 8. Deffrasnes C, Marsh GA, Foo CH, Rootes CL, Gould CM, Grusovin J, et al. Genome-wide
800 siRNA Screening at Biosafety Level 4 Reveals a Crucial Role for Fibrillarin in Henipavirus
801 Infection. PLoS Pathog. 2016;12(3):e1005478. doi: 10.1371/journal.ppat.1005478. PubMed
802 PMID: 27010548; PubMed Central PMCID: PMCPMC4806981.

803 9. Monaghan P, Green D, Pallister J, Klein R, White J, Williams C, et al. Detailed
804 morphological characterisation of Hendra virus infection of different cell types using super-
805 resolution and conventional imaging. Virol J. 2014;11:200. doi: 10.1186/s12985-014-0200-5.
806 PubMed PMID: 25428656; PubMed Central PMCID: PMCPMC4254186.

807 10. Pentecost M, Vashisht AA, Lester T, Voros T, Beaty SM, Park A, et al. Evidence for
808 ubiquitin-regulated nuclear and subnuclear trafficking among Paramyxovirinae matrix proteins.
809 PLoS Pathog. 2015;11(3):e1004739. doi: 10.1371/journal.ppat.1004739. PubMed PMID:
810 25782006; PubMed Central PMCID: PMCPMC4363627.

811 11. Wang YE, Park A, Lake M, Pentecost M, Torres B, Yun TE, et al. Ubiquitin-regulated
812 nuclear-cytoplasmic trafficking of the Nipah virus matrix protein is important for viral budding.
813 PLoS Pathog. 2010;6(11):e1001186. doi: 10.1371/journal.ppat.1001186. PubMed PMID:
814 21085610; PubMed Central PMCID: PMCPMC2978725.

815 12. Battisti AJ, Meng G, Winkler DC, McGinnes LW, Plevka P, Steven AC, et al. Structure
816 and assembly of a paramyxovirus matrix protein. Proc Natl Acad Sci U S A. 2012;109(35):13996-
817 4000. Epub 2012/08/15. doi: 10.1073/pnas.1210275109. PubMed PMID: 22891297; PubMed
818 Central PMCID: PMCPMC3435216.

819 13. Liu YC, Grusovin J, Adams TE. Electrostatic Interactions between Hendra Virus Matrix
820 Proteins Are Required for Efficient Virus-Like-Particle Assembly. J Virol. 2018;92(13). Epub
821 2018/04/27. doi: 10.1128/JVI.00143-18. PubMed PMID: 29695428; PubMed Central PMCID:
822 PMCPMC6002731.

823 14. Rawlinson SM, Zhao T, Rozario AM, Rootes CL, McMillan PJ, Purcell AW, et al. Viral
824 regulation of host cell biology by hijacking of the nucleolar DNA-damage response. Nat Commun.
825 2018;9(1):3057. Epub 2018/08/05. doi: 10.1038/s41467-018-05354-7. PubMed PMID: 30076298;
826 PubMed Central PMCID: PMCPMC6076271.

827 15. Sun W, McCrory TS, Khaw WY, Petzing S, Myers T, Schmitt AP. Matrix proteins of
828 Nipah and Hendra viruses interact with beta subunits of AP-3 complexes. J Virol.
829 2014;88(22):13099-110. doi: 10.1128/JVI.02103-14. PubMed PMID: 25210190; PubMed Central
830 PMCID: PMCPMC4249102.

831 16. Donnelly CM, Vogel OA, Edwards MR, Taylor PE, Roby JA, Forwood JK, et al.
832 Henipavirus Matrix Protein Employs a Non-Classical Nuclear Localization Signal Binding
833 Mechanism. Viruses. 2023;15(6). Epub 2023/06/28. doi: 10.3390/v15061302. PubMed PMID:
834 37376602; PubMed Central PMCID: PMCPMC10303457.

835 17. McLinton EC, Wagstaff KM, Lee A, Moseley GW, Marsh GA, Wang LF, et al. Nuclear
836 localization and secretion competence is conserved amongst henipavirus matrix proteins. J Gen
837 Virol. 2017. doi: 10.1099/jgv.0.000703. PubMed PMID: 28056216.

838 18. Watkinson RE, Lee B. Nipah virus matrix protein: expert hacker of cellular machines.
839 FEBS Lett. 2016;590(15):2494-511. doi: 10.1002/1873-3468.12272. PubMed PMID: 27350027.

840 19. Liang SH, Clarke MF. Regulation of p53 localization. Eur J Biochem. 2001;268(10):2779-
841 83. Epub 2001/05/19. doi: 10.1046/j.1432-1327.2001.02227.x. PubMed PMID: 11358492.

842 20. Gorby C, Martinez-Fabregas J, Wilmes S, Moraga I. Mapping Determinants of Cytokine
843 Signaling via Protein Engineering. Front Immunol. 2018;9:2143. Epub 2018/10/16. doi:
844 10.3389/fimmu.2018.02143. PubMed PMID: 30319612; PubMed Central PMCID:
845 PMCPMC6170656.

846 21. Banani SF, Lee HO, Hyman AA, Rosen MK. Biomolecular condensates: organizers of
847 cellular biochemistry. Nat Rev Mol Cell Biol. 2017;18(5):285-98. Epub 2017/02/23. doi:
848 10.1038/nrm.2017.7. PubMed PMID: 28225081; PubMed Central PMCID: PMCPMC7434221.

849 22. Boeynaems S, Alberti S, Fawzi NL, Mittag T, Polymenidou M, Rousseau F, et al. Protein
850 Phase Separation: A New Phase in Cell Biology. Trends Cell Biol. 2018;28(6):420-35. Epub
851 2018/04/01. doi: 10.1016/j.tcb.2018.02.004. PubMed PMID: 29602697; PubMed Central PMCID:
852 PMCPMC6034118.

853 23. Rawlinson SM, Zhao T, Ardipradja K, Zhang Y, Veugelers PF, Harper JA, et al.
854 Henipaviruses and lyssaviruses target nucleolar treacle protein and regulate ribosomal RNA

855 synthesis. Traffic. 2023;24(3):146-57. Epub 2022/12/09. doi: 10.1111/tra.12877. PubMed PMID:
856 36479968.

857 24. Larsen DH, Hari F, Clapperton JA, Gwerder M, Gutsche K, Altmeyer M, et al. The NBS1-
858 Treacle complex controls ribosomal RNA transcription in response to DNA damage. Nat Cell Biol.
859 2014;16(8):792-803. doi: 10.1038/ncb3007. PubMed PMID: 25064736; PubMed Central PMCID:
860 PMCPMC4962910.

861 25. So RB, Gonzales B, Henning D, Dixon J, Dixon MJ, Valdez BC. Another face of the
862 Treacher Collins syndrome (TCOF1) gene: identification of additional exons. Gene. 2004;328:49-
863 57. Epub 2004/03/17. doi: 10.1016/j.gene.2003.11.027. PubMed PMID: 15019983.

864 26. Ditlev JA, Case LB, Rosen MK. Who's In and Who's Out-Compositional Control of
865 Biomolecular Condensates. J Mol Biol. 2018;430(23):4666-84. Epub 2018/08/14. doi:
866 10.1016/j.jmb.2018.08.003. PubMed PMID: 30099028; PubMed Central PMCID:
867 PMCPMC6204295.

868 27. Emmott E, Hiscox JA. Nucleolar targeting: the hub of the matter. EMBO Rep.
869 2009;10(3):231-8. doi: 10.1038/embor.2009.14. PubMed PMID: 19229283; PubMed Central
870 PMCID: PMCPMC2658561.

871 28. Luo YY, Wu JJ, Li YM. Regulation of liquid-liquid phase separation with focus on post-
872 translational modifications. Chem Commun (Camb). 2021;57(98):13275-87. Epub 2021/11/25.
873 doi: 10.1039/d1cc05266g. PubMed PMID: 34816836.

874 29. Mohanty P, Kapoor U, Sundaravadivelu Devarajan D, Phan TM, Rizuan A, Mittal J.
875 Principles Governing the Phase Separation of Multidomain Proteins. Biochemistry. 2022. Epub
876 2022/07/09. doi: 10.1021/acs.biochem.2c00210. PubMed PMID: 35802394.

877 30. Conti BA, Oppikofer M. Biomolecular condensates: new opportunities for drug discovery
878 and RNA therapeutics. Trends Pharmacol Sci. 2022;43(10):820-37. Epub 2022/08/27. doi:
879 10.1016/j.tips.2022.07.001. PubMed PMID: 36028355.

880 31. Mitrea DM, Mittasch M, Gomes BF, Klein IA, Murcko MA. Modulating biomolecular
881 condensates: a novel approach to drug discovery. Nat Rev Drug Discov. 2022;21(11):841-62.
882 Epub 2022/08/17. doi: 10.1038/s41573-022-00505-4. PubMed PMID: 35974095; PubMed Central
883 PMCID: PMCPMC9380678 discovery company that studies condensates, and have a financial
884 stake in the company.

885 32. Risso-Ballester J, Galloux M, Cao J, Le Goffic R, Hontonnou F, Jobart-Malfait A, et al. A
886 condensate-hardening drug blocks RSV replication in vivo. Nature. 2021;595(7868):596-9. Epub
887 2021/07/09. doi: 10.1038/s41586-021-03703-z. PubMed PMID: 34234347.

888 33. Wang S, Dai T, Qin Z, Pan T, Chu F, Lou L, et al. Targeting liquid-liquid phase separation
889 of SARS-CoV-2 nucleocapsid protein promotes innate antiviral immunity by elevating MAVS
890 activity. Nat Cell Biol. 2021;23(7):718-32. Epub 2021/07/10. doi: 10.1038/s41556-021-00710-0.
891 PubMed PMID: 34239064.

892 34. Maehama T, Nishio M, Otani J, Mak TW, Suzuki A. Nucleolar stress: Molecular
893 mechanisms and related human diseases. Cancer Sci. 2023;114(5):2078-86. Epub 2023/02/11. doi:
894 10.1111/cas.15755. PubMed PMID: 36762786; PubMed Central PMCID: PMCPMC10154868.

895 35. Stochaj U, Weber SC. Nucleolar Organization and Functions in Health and Disease. Cells.
896 2020;9(3). Epub 2020/02/29. doi: 10.3390/cells9030526. PubMed PMID: 32106410; PubMed
897 Central PMCID: PMCPMC7140423.

898 36. Stewart CR, Marsh GA, Jenkins KA, Gantier MP, Tizard ML, Middleton D, et al.
899 Promotion of Hendra virus replication by microRNA 146a. J Virol. 2013;87(7):3782-91. Epub
900 2013/01/25. doi: 10.1128/JVI.01342-12. PubMed PMID: 23345523; PubMed Central PMCID:
901 PMCPMC3624204.

902 37. Frank D, Garnish SE, Sandow JJ, Weir A, Liu L, Clayer E, et al. Ubiquitylation of RIPK3
903 beyond-the-RHIM can limit RIPK3 activity and cell death. iScience. 2022;25(7):104632. Epub
904 2022/07/09. doi: 10.1016/j.isci.2022.104632. PubMed PMID: 35800780; PubMed Central
905 PMCID: PMCPMC9254354.

906 38. Mooser C, Symeonidou IE, Leimbacher PA, Ribeiro A, Shorrocks AK, Jungmichel S, et
907 al. Treacle controls the nucleolar response to rDNA breaks via TOPBP1 recruitment and ATR
908 activation. Nat Commun. 2020;11(1):123. Epub 2020/01/09. doi: 10.1038/s41467-019-13981-x.
909 PubMed PMID: 31913317; PubMed Central PMCID: PMCPMC6949271.

910 39. Ciccia A, Huang JW, Izhar L, Sowa ME, Harper JW, Elledge SJ. Treacher Collins
911 syndrome TCOF1 protein cooperates with NBS1 in the DNA damage response. Proc Natl Acad

912 Sci U S A. 2014;111(52):18631-6. doi: 10.1073/pnas.1422488112. PubMed PMID: 25512513;
913 PubMed Central PMCID: PMCPMC4284564.

914 40. Whelan DR, Bell TD. Image artifacts in single molecule localization microscopy: why
915 optimization of sample preparation protocols matters. Sci Rep. 2015;5:7924. doi:
916 10.1038/srep07924. PubMed PMID: 25603780; PubMed Central PMCID: PMCPMC4300460.

917 41. Rozario AM, Zwettler F, Duwé S, Hargeaves RB, Brice A, Dedecker P, et al. 'Live and
918 large': super-resolution optical fluctuation imaging (SOFI) and expansion microscopy (ExM) of
919 microtubule remodelling by rabies virus P protein. Aust J Chem. 2020;73(8):686-92.

920 42. Wolter S, Loschberger A, Holm T, Aufmkolk S, Dabauvalle MC, van de Linde S, et al.
921 rapidSTORM: accurate, fast open-source software for localization microscopy. Nat Methods.
922 2012;9(11):1040-1. doi: 10.1038/nmeth.2224. PubMed PMID: 23132113.

923

924

925 **SUPPLEMENTARY FIGURE LEGENDS**

926

927 **Figure S1. GFP-HeV M protein accumulation colocalizes with FC-DFC marker UBF1 but**
928 **not GC markers.**

929 HeLa cells were transfected to express GFP-HeV M and fixed at 24 h p.t. with 4%
930 paraformaldehyde before immunostaining for the nucleolar markers UBF1 (FC-DFC localization)
931 and NPM1 and nucleolin (GC localization). Yellow boxes are magnified in the zoom panel.
932 Hoechst 33342 (blue) was used to identify DNA/nuclei.

933

934 **Figure S2. FLAG-HeV M binds Treacle and localizes to sub-nucleolar compartments.** (A)
935 HeLa cells transfected to express FLAG-HeV M were fixed with 4% paraformaldehyde and treated
936 with or without proteinase K, before immunostaining for FLAG (green) and Treacle (red). Yellow
937 boxes are shown magnified in the zoom panel. Hoechst 33342 (blue) was used to identify
938 DNA/nuclei. (B) 293 FLP-In™ cells stably transfected to enable inducible expression of 3xFLAG-
939 HeV M or 3xFLAG-HeV M-K258A were treated with tetracycline (+Tet) to induce expressions,
940 or not treated (-Tet), for 24 h before lysis and IP for FLAG; IPs were analysed by IB using the
941 indicated antibodies.

942

943 **Figure S3. FC-DFC accumulation of NiV M protein decreases over time.**

944 (A) HeLa cells transfected to express GFP-NiV M WT or K258A proteins were analyzed live at
945 8, 16, 24, 48, and 72 h p.t. by CLSM. Images representative of major phenotypes are shown for
946 each condition, with yellow boxes magnified in the zoom panel.

947 (B) Images such as those in (A) were used to determine the percentage of cells with apparent FC-
948 DFC accumulation. The number of cells analyzed to determine the percentage for each sample is
949 indicated on the graph. n ≥ 18 cells were analysed for each time point.
950
951 **Figure S4. Inhibition of rRNA biogenesis by HeV M protein correlates with dynamic**
952 **localization to FC-DFC.** HeLa cells were transfected to express the indicated proteins before
953 addition of EU reagent. Sample were labeled to detect nascent RNA (EU fluorescence) and imaged
954 by CLSM. EU fluorescence in the nucleoli of GFP-positive cells relative to that in non-GFP
955 expressing cells in the same sample (mean relative EU fluorescence ± S.E.M., n ≥ 22 cells) ** $p<$
956 0.01; ns, non-significant.
957
958

Figure 1

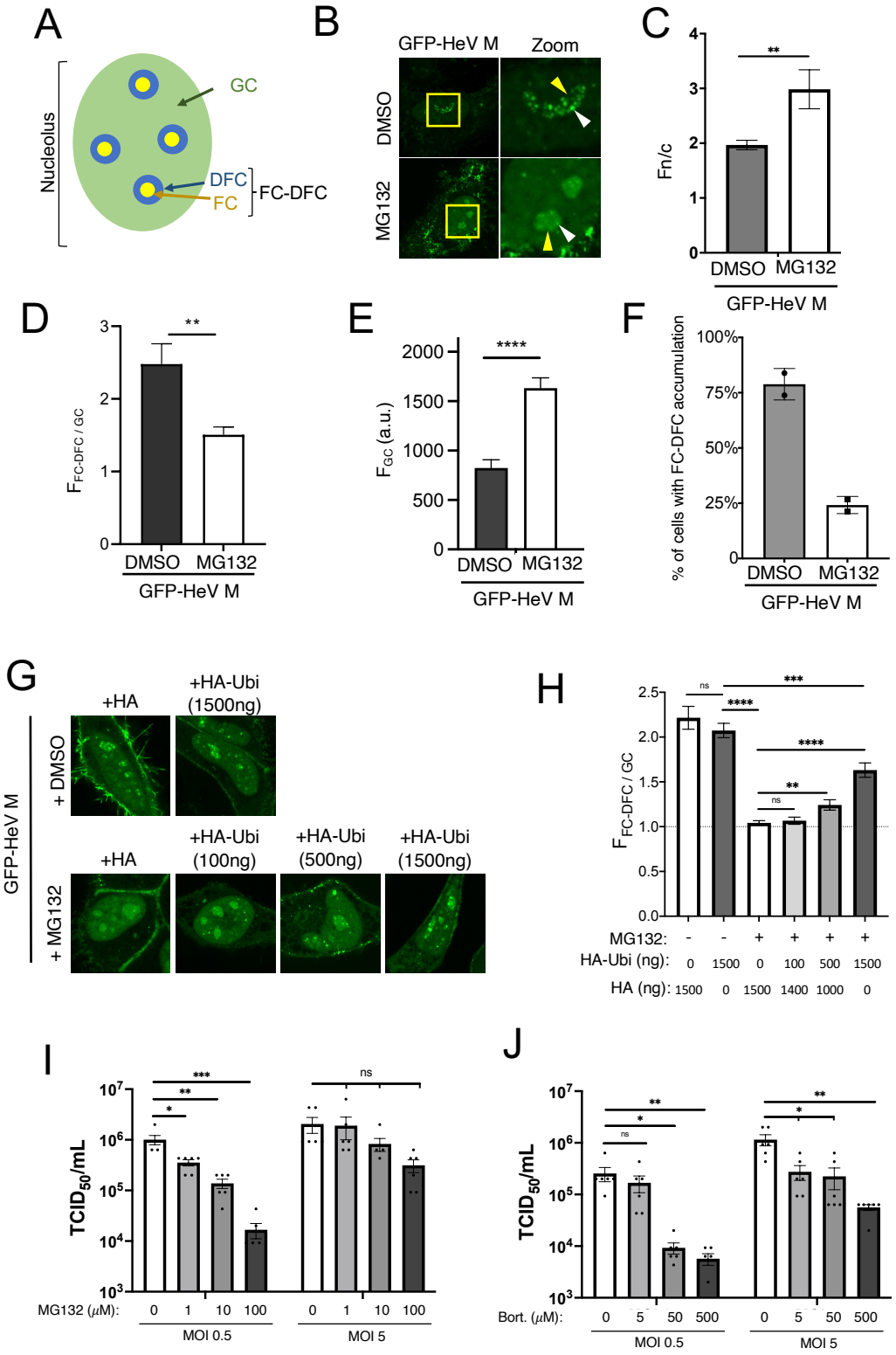
A
Nucleolus
GC
DFC
FC
FC-DFC
B
GFP-HeV M
Zoom
DMSO
MG132
C
Fn/c
DMSO
MG132
GFP-HeV M
D
$F_{FC-DFC / GC}$
DMSO
MG132
GFP-HeV M
E
F_{GC} (a.u.)
DMSO
MG132
GFP-HeV M
F
% of cells with FC-DFC accumulation
DMSO
MG132
GFP-HeV M
G
GFP-HeV M
+ DMSO
+ MG132
+HA
+HA-Ubi (1500ng)
+HA-Ubi (100ng)
+HA-Ubi (500ng)
H
$F_{FC-DFC / GC}$
MG132:
HA-Ubi (ng):
HA (ng):
I
$TCID_{50}$/mL
MG132 (μM):
MOI 0.5
MOI 5
J
$TCID_{50}$/mL
Bort. (μM):
MOI 0.5
MOI 5

Figure 2

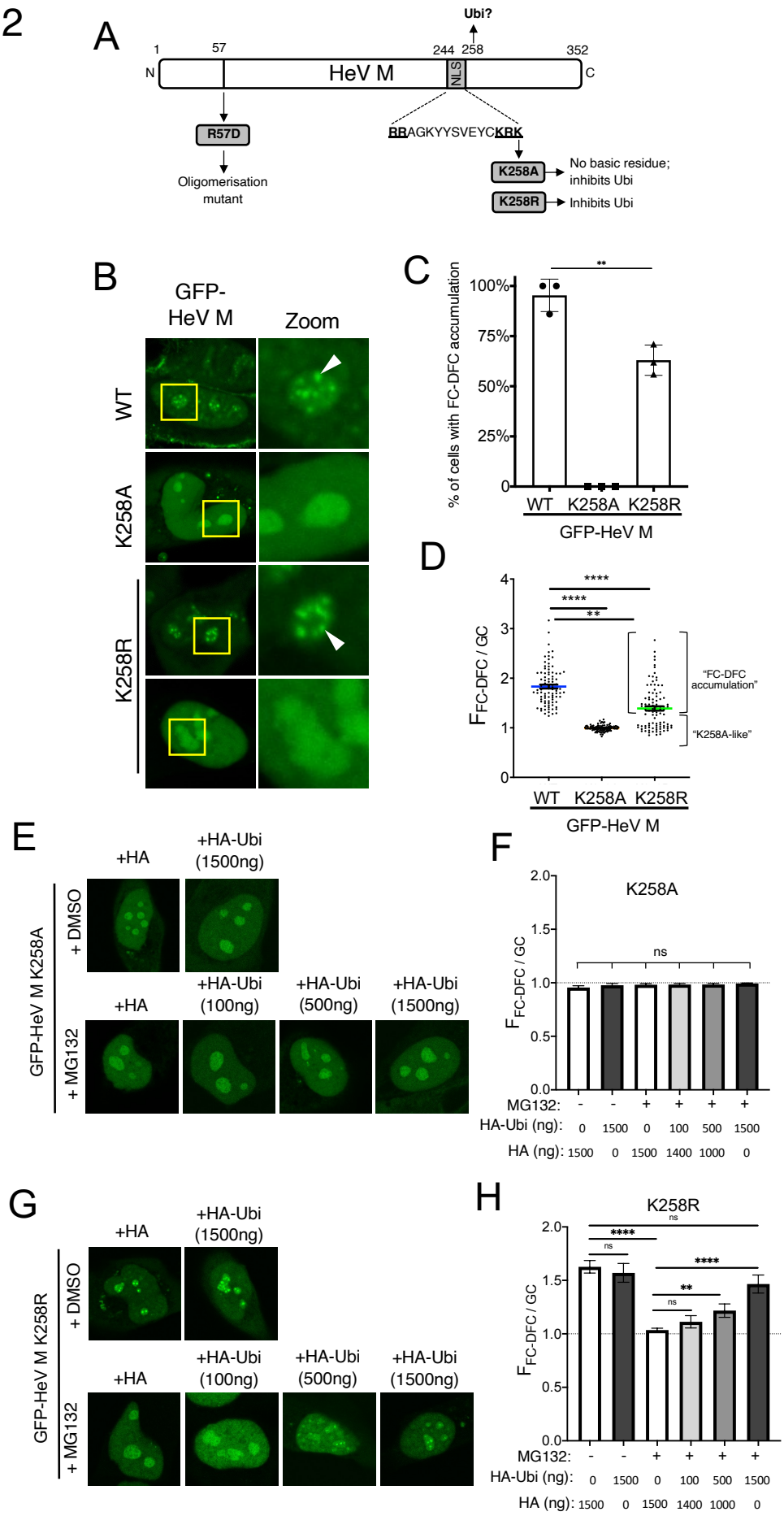
A
Ubi?
1
57
244
258
352
N
HeV M
NLS
C
R57D
Oligomerisation mutant
RRAGKYYSVEYCKRK
K258A
No basic residue; inhibits Ubi
K258R
Inhibits Ubi
B
GFP-HeV M
Zoom
WT
K258A
K258R
C
% of cells with FC-DFC accumulation
100%
75%
50%
25%
0
**
WT
K258A
K258R
GFP-HeV M
D
F_{FC-DFC} / GC
4
3
2
1
0
****
****
**
"FC-DFC accumulation"
"K258A-like"
WT
K258A
K258R
GFP-HeV M
E
+HA
+HA-Ubi (1500ng)
GFP-HeV M K258A
+ DMSO
+ MG132
+HA
+HA-Ubi (100ng)
+HA-Ubi (500ng)
+HA-Ubi (1500ng)
F
K258A
F_{FC-DFC} / GC
2.0
1.5
1.0
0.5
0.0
ns
MG132: - - + + + +
HA-Ubi (ng): 0 1500 0 100 500 1500
HA (ng): 1500 0 1500 1400 1000 0
G
+HA
+HA-Ubi (1500ng)
GFP-HeV M K258R
+ DMSO
+ MG132
+HA
+HA-Ubi (100ng)
+HA-Ubi (500ng)
+HA-Ubi (1500ng)
H
K258R
F_{FC-DFC} / GC
2.0
1.5
1.0
0.5
0.0
ns
****
ns
****
**
ns
MG132: - - + + + +
HA-Ubi (ng): 0 1500 0 100 500 1500
HA (ng): 1500 0 1500 1400 1000 0

Figure 3

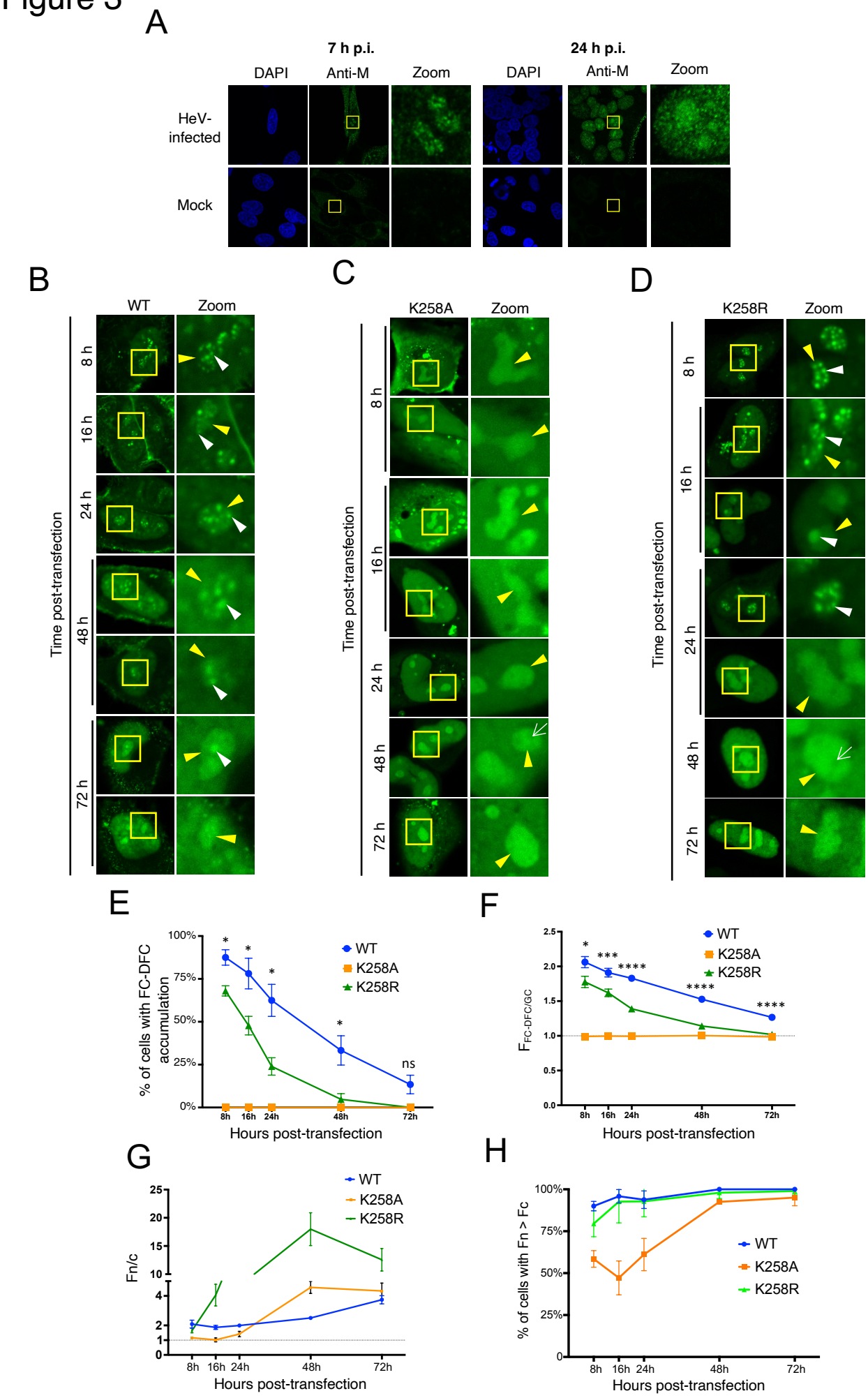
A
7 h p.i.
24 h p.i.
DAPI
Anti-M
Zoom
HeV-infected
Mock
B
WT
Zoom
Time post-transfection
8 h
16 h
24 h
48 h
72 h
C
K258A
D
K258R
E
% of cells with FC-DFC accumulation
Hours post-transfection
WT
K258A
K258R
ns
F
$F_{FC-DFC/GC}$
G
Fn/c
H
% of cells with Fn > Fc

Figure 4

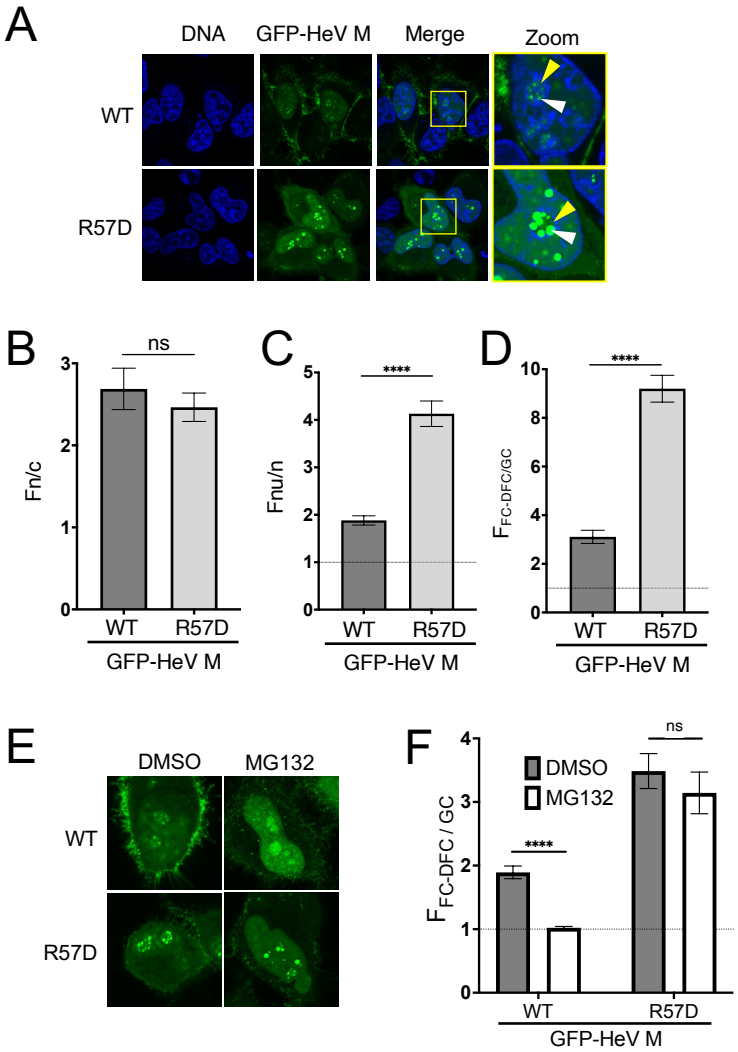
A
DNA
GFP-HeV M
Merge
Zoom
WT
R57D
B
ns
Fn/c
WT
R57D
GFP-HeV M
C
****
Fnu/n
WT
R57D
GFP-HeV M
D
****
$F_{FC-DFC/GC}$
WT
R57D
GFP-HeV M
E
DMSO
MG132
WT
R57D
F
DMSO
MG132
ns
****
F_{FC-DFC} / GC
WT
R57D
GFP-HeV M

Figure 5

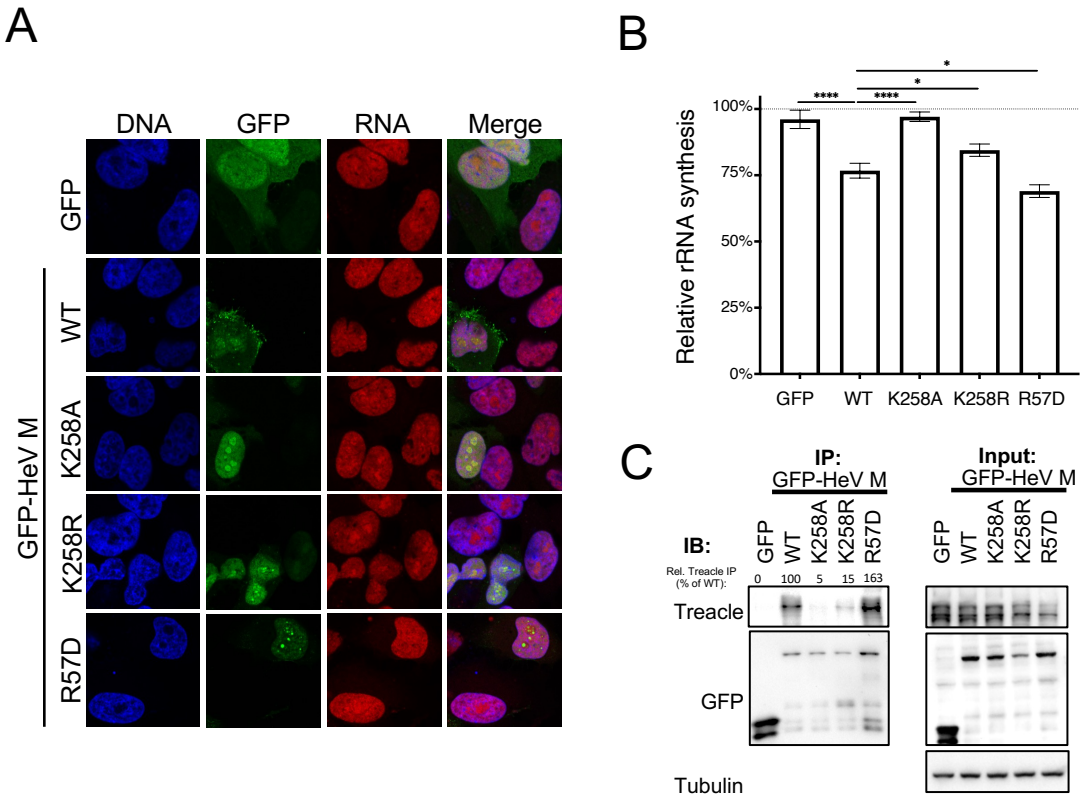
A
DNA
GFP
RNA
Merge
GFP
GFP-HeV M
WT
K258A
K258R
R57D
B
Relative rRNA synthesis
100%
75%
50%
25%
0%
****
****
*
*
GFP
WT
K258A
K258R
R57D
C
IP:
GFP-HeV M
Input:
GFP-HeV M
IB:
GFP
WT
K258A
K258R
R57D
Rel. Treacle IP
(% of WT):
0
100
5
15
163
Treacle
GFP
Tubulin

Figure 6

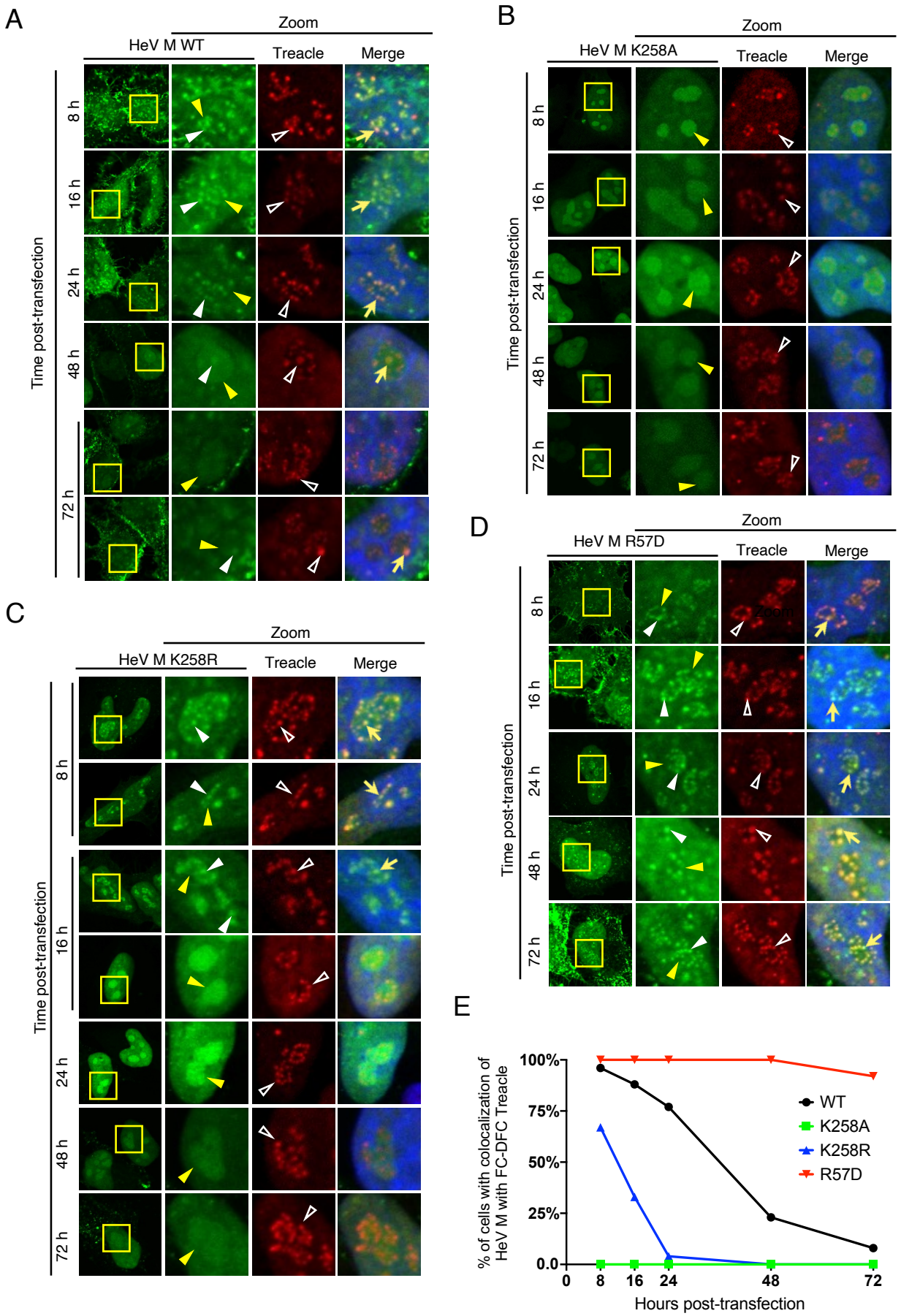
A
Zoom
HeV M WT
Treacle
Merge
Time post-transfection
8 h
16 h
24 h
48 h
72 h
B
Zoom
HeV M K258A
Treacle
Merge
Time post-transfection
8 h
16 h
24 h
48 h
72 h
C
Zoom
HeV M K258R
Treacle
Merge
Time post-transfection
8 h
16 h
24 h
48 h
72 h
D
Zoom
HeV M R57D
Treacle
Merge
Time post-transfection
8 h
16 h
24 h
48 h
72 h
E
% of cells with colocalization of HeV M with FC-DFC Treacle
100%
75%
50%
25%
0.0
0
8
16
24
48
72
Hours post-transfection
WT
K258A
K258R
R57D

Figure 7

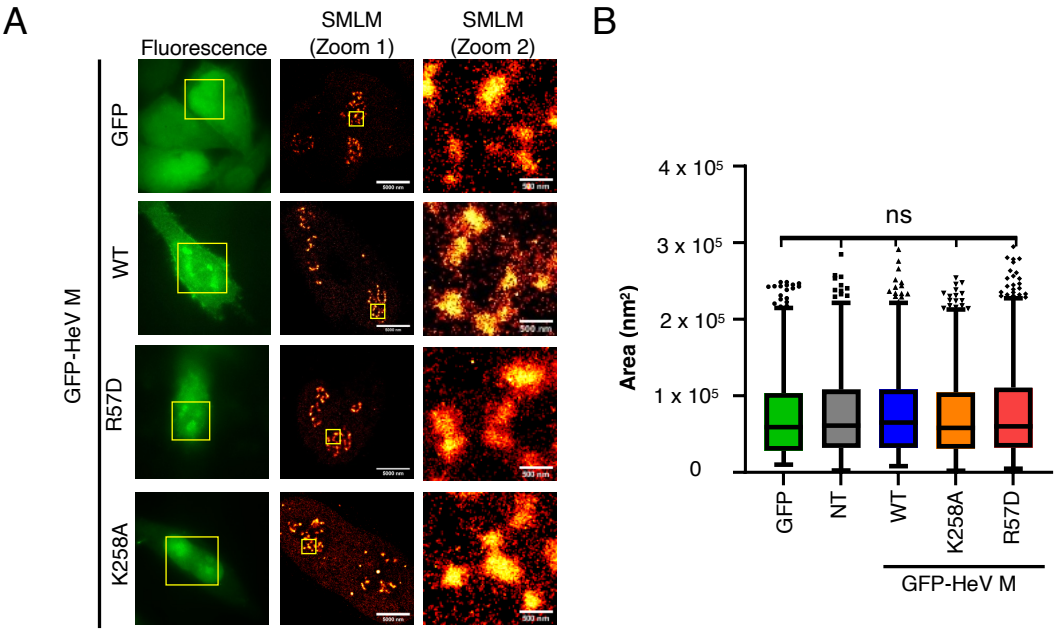
A
Fluorescence
SMLM (Zoom 1)
SMLM (Zoom 2)
GFP-HeV M
GFP
WT
R57D
K258A
B
Area (nm²)
4 x 10⁵
3 x 10⁵
2 x 10⁵
1 x 10⁵
0
ns
GFP
NT
WT
K258A
R57D
GFP-HeV M

Figure 8

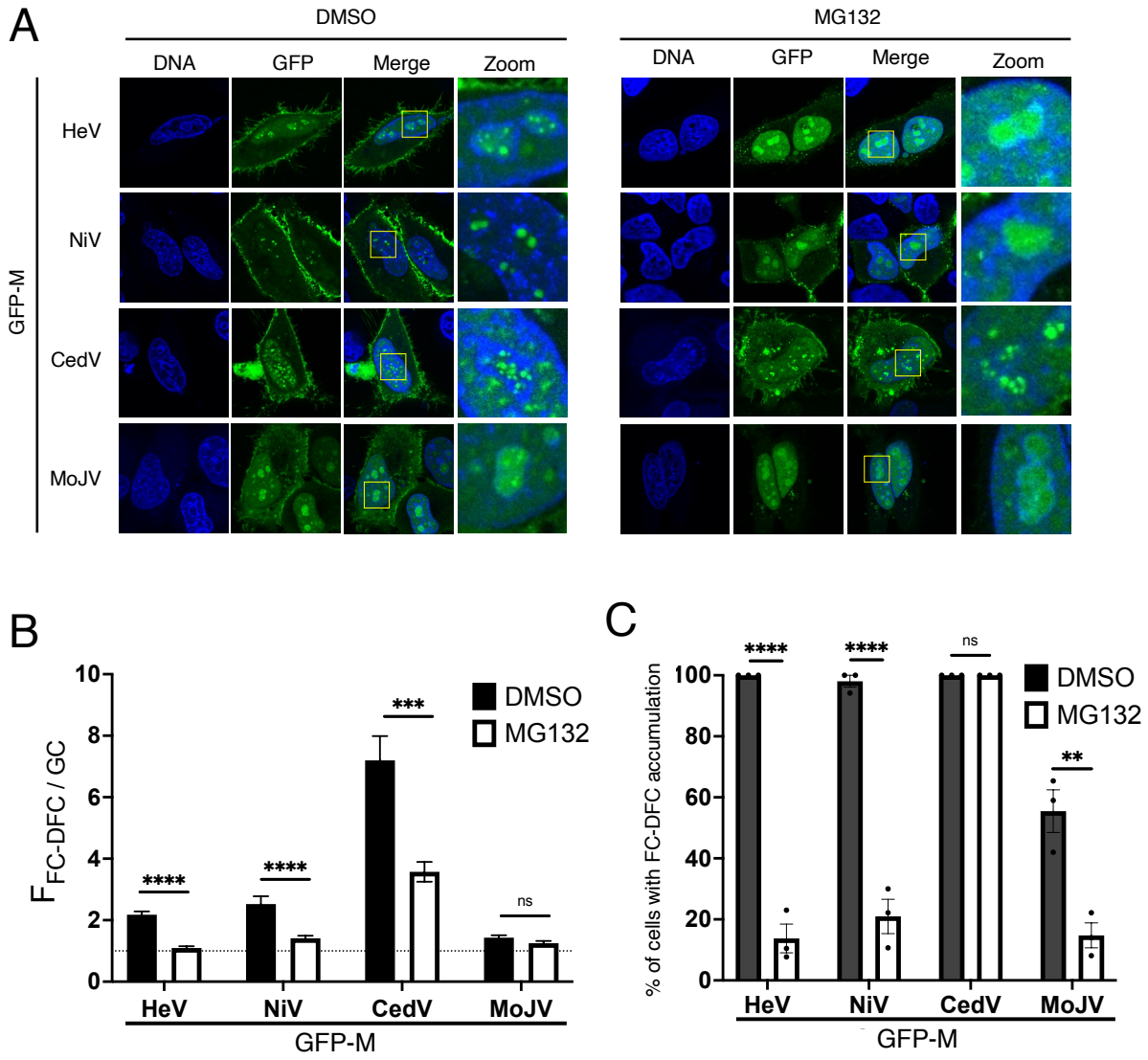
A
DMSO
MG132
DNA
GFP
Merge
Zoom
GFP-M
HeV
NiV
CedV
MoJV
B
$F_{FC-DFC / GC}$
DMSO
MG132
****
****
***
ns
HeV
NiV
CedV
MoJV
GFP-M
C
% of cells with FC-DFC accumulation
****
****
ns
**
HeV
NiV
CedV
MoJV
GFP-M